Topographically Directed Nucleation of Organic Crystals on Molecular Single-Crystal Substrates

Phillip W. Carter and Michael D. Ward*

Contribution from the Department of Chemical Engineering and Materials Science, University of Minnesota, Minneapolis, Minnesota 55455-0132

Received April 19, 1993®

Abstract: The role of specific crystal planes of single crystals of β-succinic acid (sa) and L-valine (val) as substrates for the nucleation and growth of organic crystals has been examined. Freshly cleaved crystals of these substrates provide flat terraces and ledge sites corresponding to planes whose molecular structures are well-defined by the crystallographic structure of the substrate. Nucleation of benzoic acid on these substrates occurs at low driving force at $[10\bar{1}]_{sa}$ and $[010]_{val}$ ledge sites formed from pairs of planes identified by atomic force microscopy as $(0\bar{1}0)_{sa} \cap (1\bar{1}1)_{sa}$ and $(001)_{val} \cap (\bar{2}01)_{val}$, respectively. Growth from these ledge sites is attributed to lowering of the prenucleation aggregate free energy via "ledge directed epitaxy" that involves a lattice match between the substrate and growing phase along the ledge direction, and equivalent dihedral angles of the substrate ledge sites and a pair of aggregate planes whose identity is assigned on the basis of the structure of the mature crystal. For example, the $[10\bar{1}]_{sa}$ ledge has a 1.0% lattice mismatch with the [110] direction of benzoic acid and a difference of only 0.6° between the ledge dihedral angle and the dihedral angle of the $(001)_{ba} \cap (1\bar{1}2)_{ba}$ planes. On the basis of the crystal structures, these interfaces consist of "molecularly smooth" low-energy planes, consistent with stabilization of the prenucleation aggregates by dispersive interactions. As a consequence of these epitaxial effects and the crystallographic symmetry of the monoclinic space groups of the substrates and benzoic acid, benzoic acid growth is highly oriented. Oriented growth of 4-nitroaniline (pna) crystals is also observed on $[10\bar{1}]_{sa}$ and $[010]_{val}$ ledge sites, with $[10\bar{1}]_{pna}$, the direction containing hydrogen-bonded 4-nitroaniline chains, aligned along the ledge directions. In each case, the lattice mismatch along the ledge direction is small and stabilization of the prenucleation aggregate by interaction with both planes of the ledge is evident from the absence of nucleation on ledge-free areas of the substrates. Experimental observations and calculations suggest that topographically directed growth orientation is observed when aggregate adsorption at the ledge is dominated by dispersive forces. Smaller contributions from dipolar and hydrogen bonding interactions may also play a role in nucleation of 4-nitroaniline on L-valine, in which 4-nitroaniline chains align with the polar $[010]_{val}$ axis of the substrate ledge. These studies indicate that generally accepted epitaxy concepts involving principal lattice directions of the substrate and growing phase may be an oversimplified explanation of crystal growth on crystalline substrates. Rather, nucleation of crystalline phases on molecular crystal substrates is controlled by topographic structure, lattice parameters of ledge nucleation sites, symmetry constraints, and molecular composition of aggregate and substrate crystal planes.

Introduction

Crystalline solids based on molecular components exhibit numerous properties of fundamental and technological interest, including electrical conductivity, superconductivity, nonlinear optical behavior, and ferromagnetism.[1] The principal advantage of these materials is the ability to rationally control bulk properties through molecular design, which requires a thorough understanding of the factors responsible for the supramolecular structure of molecular crystals. Accordingly, "crystal engineering" strategies based on the design of thermodynamically preferred intermolecular interactions in the bulk crystal have developed.[2] However, relatively little effort has been spent examining the formation of molecular crystals in the context of the nucleation and crystal growth *process*. This is in stark contrast to extensive investigations of the crystal growth mechanisms of ice,[3] inorganic, and elemental systems,[4] although these studies rarely explore these mechanisms from a molecular perspective.

Crystal growth of a molecular crystal can be described as a stepwise self-assembly process in which molecules form very small prenucleation aggregates, which then form nuclei that grow into macroscopic crystals. It is commonly accepted that the supramolecular structure of the prenucleation aggregates resembles the crystal structure of the mature crystalline phase.[5] Therefore, control of the structure of prenucleation aggregates could lead to directed self-assembly of molecular components into nuclei and crystals with preordained supramolecular structures, possibly including kinetically preferred metastable polymorphs. Since nucleation almost always occurs at heterogeneous or solid interfaces due to the lowering of the surface energy of prenucleation aggregates and crystal nuclei, the structure of a substrate interface can play an important role in the crystallization pathway.

Limited studies of growth of molecular crystals at interfaces have appeared, including observations of oriented growth on polymeric[6] and ionic substrates[7] and epitaxy on semiconductor

* To whom correspondence should be addressed.

® Abstract published in *Advance ACS Abstracts*, November 1, 1993.

(1) Miller, J. S., Ed. *Extended Linear Chain Compounds*; Plenum Press: New York.

(2) (a) Schmidt, G. M. J. *Pure Appl. Chem.* **1971**, *27*, 647. (b) Desiraju, G. R. *Crystal Engineering—The Design of Organic Solids*; Elsevier: New York, 1989. (c) Etter, M. C. *Acc. Chem. Res.* **1990**, *23*, 120.

(3) (a) Evans, L. F. *Nature* **1965**, *206*, 822. (b) Evans, L. F. *Nature* **1967**, 384. (c) Edwards, G. R.; Evans, L. F. *Nature* **1961**, *192*, 448. (d) Vonnegut, B. *J. Appl. Phys.* **1947**,*18*, 593. (e) Blair, D. N.; Davis, B. L.; Dennis, A. S. *J. Appl. Meteorol.* **1973**, *12*, 1012. (f) Davis, B. L; Johnson, L. R; Moeng, F. J. *J. Appl. Meteorol.* **1975**, *14*, 891.

(4) (a) Brice, J. C. *Crystal Growth Processes*, John Wiley and Sons: New York, 1986. (b) Hartman, P., Ed. *Crystal Growth: An introduction*; North Holland: Amsterdam, 1973.

(5) Addadi, L.; Berkovitch-Yellin, Z.; Weissbuch, I.; van Mil, J.; Shimon, L. J. W.; Lahav, M.; Leiserowitz, L. *Angew. Chem., Int Ed. Engl.* **1985**, *24*, 466.

0002-7863/93/1515-11521$04.00/0

substrates.[8] Investigations of the nucleation and growth of amino acids[9] and inorganic compounds[10,11] beneath Langmuir monolayers and ice crystallization on alcohol monolayers on water droplets have also been reported.[12] Further advances in this area would have a significant impact on the formation of molecular crystals in which crystal growth rates, phase selectivity, and morphology issues are problematic. For example, the simultaneous growth of multiple phases has been observed during the electrochemical preparation of low-dimensional organic superconductors on solid electrodes.[13] Fundamental aspects of the commonly accepted practice of crystal seeding, which clearly involve heterogeneous crystal growth on crystal seeds, are not thoroughly understood. This is of considerable importance in the resolution of optically active enantiomers.[14,15] Control of crystal morphology is also important in pharmaceutical processing, where bioavailability, delivery of crystalline reagents, and solid flow characteristics are critical factors.[16] The preparation of non-centrosymmetric molecular crystals, necessary for second harmonic generation,[17] is difficult to achieve due to their apparent preference for centrosymmetric space groups.[18] Crystallization on properly designed solid surfaces, which intrinsically lack a center of symmetry, may favor nucleation of non-centrosymmetric crystalline phases. These issues prompted us to examine strategies for molecular level design of solid substrates capable of influencing nucleation of molecular crystals in a rational manner. The molecular surfaces employed in such a strategy may include molecular films such as Langmuir–Blodgett and self-assembled monolayers, or crystal planes of molecular crystals. The latter approach provides a unique opportunity to examine several fundamental aspects of growth, as the interfacial structure of exposed molecular crystal planes are crystallographically defined. A single crystal also can exhibit a variety of crystal planes, with different molecular structures and enantiotopic properties.

Chart I

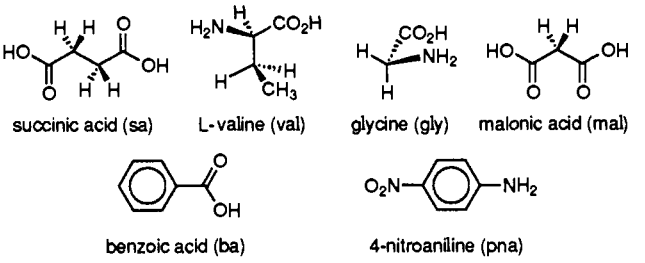

Previous studies of crystal growth on solid substrates generally have involved simple concepts of epitaxy associated with principal lattice directions contained in the interface between the substrate and growing crystalline phase.[7,8] However, recent reports of the crystallization of ice on amino acid crystals suggest that nucleation may occur in microcrevices on the surface of the single-crystal substrate,[19] a mechanism that had been ignored in previous studies of ice nucleation on amino acids.[20] Indeed, studies of epitaxial growth on single-crystal substrates generally have ignored the role of topographical features such as substrate ledges and kinks in nucleation, even though these features play an important role in single-phase crystal growth.[21]

We herein report our initial investigations of nucleation on crystal planes of different molecular crystals. These studies reveal the influence of substrate topography, lattice parameters, crystallographic symmetry, and intermolecular interactions on nucleation and growth orientation. Specifically, we describe the growth of benzoic acid and 4-nitroaniline single crystals on freshly cleaved surfaces of succinic acid, L-valine, glycine, and malonic acid substrates in which exposed crystal planes provide molecular interfaces whose structure and composition are defined by their respective crystal structures.[22] These studies indicate that nucleation of organic crystals can be strongly affected by the topography of well-defined substrate surfaces, the availability of multiple interfaces on the substrate during nucleation, and the proper geometrical relationship between these interfaces and the shape of the prenucleation aggregate. Nucleation of benzoic acid and 4-nitroaniline occurs preferentially at densely packed, "molecularly smooth" planes of substrate ledge sites where prenucleation aggregates are stabilized primarily by attractive dispersive interactions between densely-packed crystal planes of the substrate and aggregates of the growing crystalline phase. In the case of 4-nitroaniline, nucleation on the non-centrosymmetric substrate L-valine occurs with alignment of the 4-nitroaniline chains along the polar axis of the substrate, suggesting some contribution from dipolar forces. These observations provide evidence of the relationship between the structure of prenucleation aggregates and their respective mature crystalline phases, and suggest new criteria for the design of crystal growth processes.

(6) (a) Kawaguchi, A.; Okihara, T.; Katayama, K. *J. Cryst. Growth* **1990**, *99*, 1028. (b) Willems, J.; Willems, I. *Nature* **1956**, *178*, 429. (c) Kawaguchi, A. et al. *J. Cryst. Growth* **1989**, *94*, 857.

(7) (a) Mobus, M.; Schreck, M.; Karl, N. *Thin Solid Films* **1989**, *175*, 89. (b) Yanagi, H.; Takemoto, K.; Hayashi, S.; Ashida, M. *J. Cryst. Growth* **1990**, *99*, 1038. (c) Hayashi, S.; Ikuno, H.; Yanagi, H.; Ashida, M. *J. Cryst. Growth* **1992**, *123*, 35.

(8) Zimmerman, U.; Schnitzler, G.; Karl, N.; Umbach, E.; Dudde, R. *Thin Solid Films* **1989**, *175*, 85.

(9) (a) Landau, E. M.; Grayer Wolf, S.; Levanon, M.; Leiserowitz, L.; Lahav, M.; Sagiv, J. *J. Am. Chem. Soc.* **1989**, *111*, 1436. (b) Landau, E. M.; Grayer Wolf, Sagiv. J.; Deutsch, M.; Kjaer, K.; Als-Nielsen, J.; Leiserowitz, L.; Lahav, M. *Pure Appl. Chem.* **1989**, *61*, 673. (c) Weissbuch, I.; Frolow, F.; Addadi, L.; Lahav, M.; Leiserowitz, L. *J. Am. Chem. Soc.* **1990**, *112*, 7718.

(10) (a) Rajam, S.; Heywood, B. R.; Walker, J. B. A.; Mann, S.; Davey, R. J.; Birchall, J. D. *J. Chem. Soc., Faraday Trans.* **1991**, *87*, 727. (b) Heywood, B. R.; Rajam, S.; Mann, S. *J. Chem. Soc., Faraday Trans.* **1991**, *87*, 735. (c) Heywood, B. R.; Mann, S. *Langmuir* **1992**, *8*, 1492. (d) Heywood, B. R.; Mann, S. *J. Am. Chem. Soc.* **1992**, *114*, 4681. (e) Heywood, B. R.; Mann, S. *Adv. Mater.* **1992**, *4*, 278. (f) Mann, S.; Heywood, B. R.; Rajam, S.; Walker, J. B. A. *J. Phys. D: Appl. Phys.* **1991**, *24*, 154.

(11) (a) Zhao, X. K.; Yang, J.; McCormick, L. D.; Fendler, J. H. *J. Phys. Chem.* **1992**, *96*, 9933. (b) Yi, K. C.; Fendler, J. H. *Langmuir* **1990**, *6*, 1519. (c) Zhao, X. K.; Yuan, Y.; Fendler, J. H. *J. Chem. Soc., Chem. Commum.* **1990**, 1248. (d) Zhao, X. K.; Xu, S.; Fendler, J. H. *Langmuir* **1991**, *7*, 520. (e) Zhao, X. K.; Fendler, J. H. *Chem. Mater.* **1991**, 3, 168. (f) Zhao, X. K.; Fendler, J. H. *J. Phys. Chem.* **1991**, *95*, 3716. (g) Zhao, X. K.; McCormick, L. D.; Fendler, J. H. *Adv. Mater.* **1992**, *4*, 93.

(12) (a) Popovitz-Biro, R.; Lahav, M.; Leiserowitz, L. *J. Am. Chem. Soc.* **1991**, *113*, 8943. (b) Gavish, M.; Popovitz-Biro, R.; Lahav, M.; Leiserowitz, L. *Science* **1990**, *250*, 973.

(13) Montgomery, L. K.; Geiser, U.; Wang, H. H.; Beno, M. A.; Schultz, A. J.; Kini, A. M.; Carlson, K. D.; Williams, J. M.; Whitworth, J. R.; et al. *Synth. Met.* **1988**, *27*, A195.

(14) (a) Collet, A.; Brienne, M.-J.; Jacques, J. *Chem. Rev.* **1980**, *80*, 215. (b) Secor, R. M. *Chem. Rev.* **1963**, *63*, 297.

(15) (a) Kondepudi, D. K.; Kaufman, R. J.; Singh, N. *Science* **1990**, *250*, 975. (b) McBride, J. M.; Carter, R. L. *Angew. Chem., Int. Ed. Engl.* **1991**, *30*, 293.

(16) Byrn, S. R. *Solid State Chemistry of Drugs*; Academic Press: New York, 1982.

(17) (a) Williams, D. J. *Angew. Chem., Int. Ed. Engl.* **1984**, *23*, 690. (b) Chemla, D. S.; Zyss, J. S., Eds. *Nonlinear Optical Properties of Organic Molecules and Crystals*; Academic Press: Orlando, FL. (c) Oudar, J. L.; Chemla, D. S. *J. Chem. Phys.* **1977**, *66*, 2664. (d) Levine, B. F.; Bethea, C. G. *J. Chem. Phys.* **1977**, *66*, 1070. (e) Lalama, S. J.; Garito, A. F. *Phys. Rev. A* **1979**, *20*, 1179. (f) Frankenbach, G. M.; Etter, M. C. *Chem. Mater.* **1992**, *4*, 272. (g) Frankenbach, G. M.; Etter, M. C. *Chem. Mater.* **1989**, *1*, 10.

(18) (a) Kitaigorodsky, A. I. *Molecular Crystals and Molecules*; Academic Press: New York, 1973. (b) Whitesell, J. K.; Davis, R. E.; Saunders, L. L.; Wilson, R. J.; Feagins, J. P. *J. Am. Chem. Soc.* **1991**, *113*, 3267.

(19) Gavish, M.; Wang, J.-L.; Eisenstein, M.; Lahav, M.; Leiserowitz, L. *Science* **1992**, *256*, 815.

(20) (a) Parungo, F. P.; Lodge, J. P., Jr. *J. Atmos. Sci.* **1965**, *22*, 309. (b) Power, B. A.; Power, R. F. *Nature* **1962**, *194*, 1170. (c) Barthakur, N.; Maybank, D. J. *Nature* **1963**, *200*, 866.

(21) (a) Tiller, W. A. *The Science of Crystallization: Microscopic Interfacial Phenomena*; Cambridge University Press: New York, 1991, pp 327–381. (b) Tiller, W. A. *The Science of Crystallization: Macroscopic Phenomena and Defect Generation*; Cambridge University Press: New York, 1991; pp 283–427.

(22) (a) Leiserowitz, L. *Acta Crystallogr.* **1976**, *B32*, 775. (b) Kitaigorodsky, A. I. *Molecular Crystals and Molecules*; Academic Press: New York, 1973. (c) Gorbitz, C. H.; Etter, M. C. *Int. J. Peptide Protein Res.* **1992**, *39*, 93.

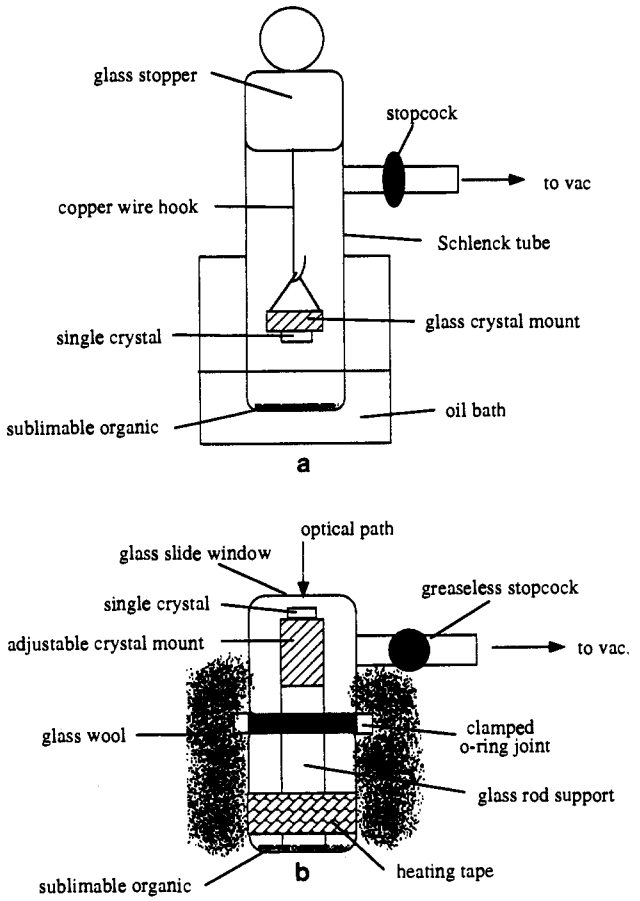

Figure 1. Schematic representation of the sublimation reactors used for (a) growth studies and (b) *in situ* PMIM studies.

Experimental Section

Materials. Succinic acid (Fluka), L-valine (Fluka), glycine (Aldrich), 4-nitroaniline (Aldrich), malonic acid (Aldrich), and benzoic acid (Mallinckrodt) were used directly without further purification. β-Succinic acid, L-valine, and α-glycine single-crystal substrates were grown by slow evaporation of saturated aqueous solutions (18 MΩ water from Barnstead E-pure water filter system), and malonic acid crystals were grown from saturated ether solutions. Millimeter-sized seed crystals were grown and then used to obtain large, single crystals with dimensions ranging from 5 to 15 mm. Substrate, nitroaniline, and benzoic acid crystals were indexed and crystal faces assigned using standard methods with an Enraf-Nonius CAD-4 diffractometer using Mo Kα radiation. In all cases, the experimental lattice parameters were in agreement with the previous reports.

Apparatus. Sublimation studies were carried out in a Schlenk tube apparatus under static vacuum (0.1 mTorr) containing single-crystal subtstrates suspended on a copper wire 4 cm. above benzoic acid or 4-nitroaniline powder (Figure 1a). Deposition times typically ranged between 2 and 120 min depending upon the temperature. The freshly cleaved faces were mounted horizontally in various orientations on the sample stage of the sublimator, and growth experiments were initiated after evacuation of the reactor.

In situ sublimation studies for optical and interferometric microscopies were performed using a glass sublimator with a 1 mm thick glass slide window sealed to the top of the cell (Figure 1b). The single-crystal surfaces were mounted 1–2 mm from the top window for interferometric measurements and approximately 1 cm from the top window for optical microscopy. The temperature was controlled with heating tape wrapped around the cell, and the entire apparatus was enclosed in glass wool. Typical operating temperatures ranged from 35 to 60 °C.

Video microscopy was performed with use of an Olympus SZH microscope (magnifications = 30–130×) equipped with a still camera and a JVC color video camera connected to a monitor and time-lapse recorder. Phase-measurement interferometric microscopy (PMIM) was performed with a Zygo Maxim-3D Model 5700 Noncontact Surface Profiler (Zygo Corp., Laurel Brook Rd., Middlefield, CT 06455). Phase measurement interferometric microscopy is a non-invasive technique capable of probing surface topography with high vertical resolution. Briefly, a laser is focused onto the sample surface and the reflected beam detected at a charge-coupled detector behind the microscope objective. The phase angle of the reflected beam is compared to a reference beam to determine the height of the sample surface under the objective. Movement of the sample in the x-y plane under the beam provides a topographic profile of the surface. Substrates were characterized in air with use of a 40× Mirau objective which provided an overall 640× magnification power and an imaging area of 245 μm × 245 μm with a lateral resolution of 0.77 μm. The maximum measurable vertical step is 158 nm, and the vertical resolution is less than 5 Å. Details of instrumentation and PMIM analysis have been presented elsewhere.[23]

Atomic force microscopy (AFM) was performed with a Digital Instruments Nanoscope III scanning probe microscope which was equipped with a d-scanner head having a 12 μm horizontal scan range to provide a greater vertical range than possible with the 0.7 μm a-scanner. AFM experiments were performed by using conical, doped silicon cantilever tips from Parc Scientific (Ultralevers) with a quoted aspect ratio of 3:1. These tips are capable of characterizing surface planes with dihedral angles greater than 105°. Scanning electron microscopy confirmed the tip geometry and aspect ratio, with the effective radius of curvature of the tip estimated to be 150 nm. The cantilever force constants of the cantilevers were typically 0.35 N/m, and surface forces ranged from 10 to 30 nN. Best results were obtained at slow scan rates (0.5 Hz) with use of low tip forces with a 1.0 V look-ahead gain on freshly cleaved surfaces. All AFM experiments were performed in air at room temperature.

Concepts of Topographically Directed Nucleation

The conceptual framework for nucleation is derived from Gibbs–Volmer theory where the free energy change for an aggregate undergoing a phase transition during homogeneous or heterogeneous nucleation is given by eq 1 where ΔG_v is the volume free energy term associated with the phase transition and ΔG_s represents the surface free energy of the aggregate.[24] For crystal growth from the gas phase a general expression for ΔG_v is given by eq 2 where j is an aggregate geometry factor, l is an aggregate length, ρ is the solid-state density, M is the molecular weight, P_s is the equilibrium vapor pressure at T, and P is the actual vapor pressure.

$$\Delta G = \Delta G_v + \Delta G_s \tag{1}$$

$$\Delta G_v = (jl^3\rho/M)RT \ln(P_s/P) \tag{2}$$

Calculation of ΔG_s for heterogenous nucleation must consider all interfaces present during the nucleation process: i.e., (1) the crystal growth medium, (2) the aggregate, and (3) the substrate. Summing up all the interfacial energy terms leads to an expression that describes the total change in surface free energy as given by eq 3,

$$\Delta G_s = \sigma_{12}S_{12} + (\sigma_{23} - \sigma_{13})S_{23} \tag{3}$$

where σ_{12}, σ_{23}, and σ_{13} are the interaction energies per unit area of the crystal growth medium–aggregate, aggregate–substrate, and medium–substrate interfaces, respectively, S_{12} is the surface area of the crystal growth medium–aggregate interface, and S_{23} is the surface area of the aggregate–substrate interface.[25] Combining eqs 1–3 provides an expression for the overall ΔG for

(23) (a) Instrumentation Information available at Zygo Corp.: Laurel Brook Road, Middlefield, CT 06455 (b) Smith, C. P.; Fritz, D. C.; Tirrell, M.; White, H. S. *Thin Solid Films* **1991**, *198*, 369. (c) Tolansky, S. *Surface Microtopography*; Interscience Publishers, Inc.: New York, 1960. (d) Tolansky, S. *Multiple-Beam Interferometry of Surfaces and Films*; Dover Publications, Inc.: New York, 1970.

(24) (a) Chalmers, B. *Principles of Solidification*; Robert E. Krieger Publishing Co.: Huntington, 1964. (b) Chakraverty, B. K. *Crystal Growth: An introduction*; Hartman, P., Ed.; North Holland: Amsterdam, 1973; pp 50–104.

(25) Fletcher, N. H. *J. Chem. Phys.* **1963**, *38*, 237.

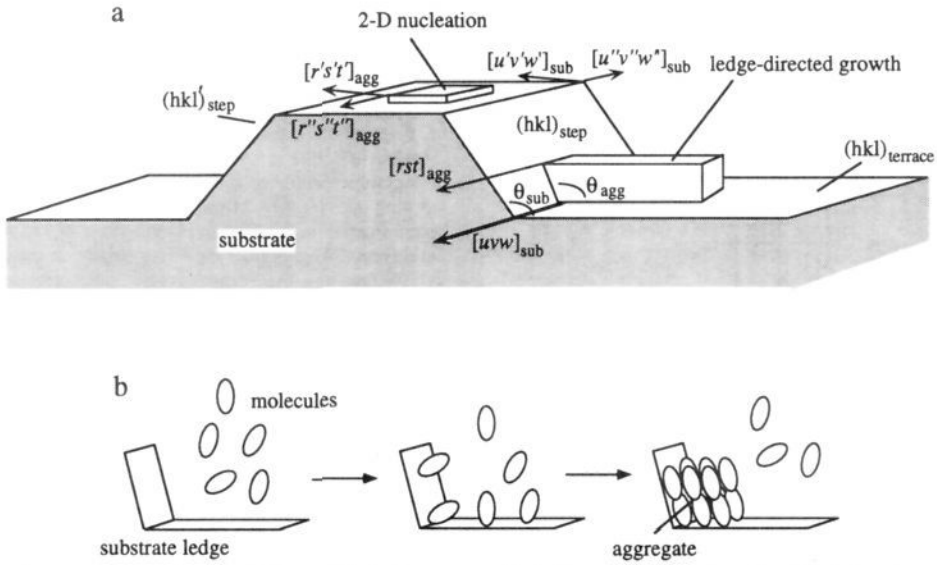

Figure 2. (a) Schematic representation of terrace, ledge, and kink sites on a generic single-crystal substrate surface. The ledge site comprises a $(hkl)_{terrace}$ and a $(hkl)_{step}$ plane, and in some cases $(hkl)'_{step}$ planes may be present on both sides of a terrace. For example, if the crystal substrate shown here has monoclinic symmetry in which the 2-fold *b*-axis is normal to the terrace, $(hkl)_{step} = (hkl)'_{step}$. Two possible crystal growth modes, two-dimensional nucleation and ledge nucleation, are shown. Since the supramolecular structure of the prenucleation aggregate must resemble the solid state structure of the mature crystal, the dimensions of the aggregate will be nearly identical to the dimensions of the crystal. Two-dimensional nucleation may involve epitaxy due to two matched lattice directions, in this case when $[r's't']_{agg} = [u'v'w']_{sub}$ and $[r''s''t'']_{agg} = [u''v''w'']_{sub}$. A ledge is denoted by its direction $[uvw]_{sub}$, and the direction of the growing aggregate that is coincident with the ledge direction is given by $[rst]_{agg}$. The dihedral angle of the ledge is defined as θ_{sub}, and the dihedral angle of a complementary pair or planes in the aggregate θ_{agg}. For the substrates examined here the following assignments apply: for succinic acid, $[uvw]_{sub} = [10\bar{1}]_{sa}$, $(hkl)_{terrace} = (0\bar{1}0)_{sa}$, $(hkl)_{step} = (111)_{sa}$, $(hkl)'_{step} = (1\bar{1}1)_{sa}$; for L-valine, $[uvw]_{sub} = [101]_{val}$, $(hkl)_{terrace} = (001)_{val}$, $(hkl)_{step} = (201)_{val}$, $(hkl)'_{step} = (\bar{2}01)_{val}$. For the growing aggregate the following assignments apply: for benzoic acid on succinic acid, $[rst]_{agg} = [110]_{ba}$; for benzoic acid on L-valine, $[rst]_{agg} = [010]_{ba}$; for 4-nitroaniline on either substrate, $[rst]_{agg} = [10\bar{1}]_{pna}$. (b) Schematic representation of nucleation at a ledge in which molecules in the gas phase adsorb on the surface and migrate to the ledge, resulting in the formation of a prenucleation aggregate at the ledge.

gas-phase heterogeneous nucleation processes (eq 4).

$$\Delta G = (jl^3\rho/M)RT\ln(P_s/P) + \sigma_{12}S_{12} + (\sigma_{23} - \sigma_{13})S_{23} \quad (4)$$

Inspection of eq 4 reveals that the overall free energy for nucleation will be lowered by a large volume free energy, a favorable surface interaction between the aggregate and the substrate (i.e., σ_{23} is negative), and an unfavorable surface energy associated with the medium–substrate interface (i.e., σ_{13} is positive). The lowering of the total surface energy upon interaction of an aggregate with the substrate is the primary reason for the predominance of heterogeneous nucleation over homogeneous nucleation. A favorable σ_{23} term can be realized by strong intermolecular interaction between the substrate and aggregate, possibly by epitaxial matching along defined crystallographic directions. If the $(\sigma_{23} - \sigma_{13})$ term in eq 4 is negative, an increase in the surface area of the aggregate–substrate interface also will serve to promote nucleation. Consequently, the nucleation of molecular crystals on foreign substrates can be enhanced if ledge sites exist which *can provide more than one surface for interfacial contact with the aggregate* (Figure 2a). This is analogous to the well-known terrace-ledge-kink (TLK) mode of crystal growth of single-phase materials,[21] in which nucleation at ledges occurs more readily than two-dimensional nucleation on terraces. This property is attributed to the greater number of nearest neighbors formed during nucleation at ledges, resulting in a greater reduction in ΔG_s, ΔG, and the critical size of the aggregate. Nucleation on the ledge sites will form kink-like crystal growth centers, with subsequent growth occurring at the kink sites parallel to the ledge, a process which is even more favorable that the initial growth at the ledge. The kinks advance toward each other at a velocity that is dependent upon the free energy change associated with the phase transition, leading to overall ledge advancement at a rate that is determined by the rates of nucleation and kink advancement. In the absence of ledges, growth can occur (although generally at higher driving forces) by less preferable modes such as two-dimensional nucleation, screw dislocations, or twin-plane reentrant corners.

Ledge nucleation and two-dimensional nucleation are schematically represented in Figure 2, which depicts a prenucleation aggregate on a crystal substrate surface possessing terraces separated by step planes. The ledge is assigned by the direction along which the terrace and step planes intersect.[26] Since the supramolecular structure of the prenucleation aggregate is the same as that of the mature crystal, the lattice constants and interplanar dihedral angles of the aggregate can be deduced from the crystal structure of the mature phase. Epitaxially driven two-dimensional nucleation may be favored if directions contained in the interface of the growing aggregate and substrate terraces (or the step planes) are equivalent, for example, if $[r's't']_{agg} = [u'v'w']_{sub}$ and $[r''s''t'']_{agg} = [u''v''w'']_{sub}$ (these directions need not be the unit cell lattice constants *a*,*b*,*c*; hence, we use a general notation here to describe the directions). However, interfacial stabilization of the prenucleation aggregate can also be realized at a ledge site when epitaxy is present along the ledge direction ($[rst]_{agg} = [uvw]_{sub}$), particularly if the geometry of the ledge is complementary to the shape of the prenucleation aggregate so that the σ_{23} term in eq 4 is favorable. That is, *nucleation will be enhanced if there are two suitable crystal planes in the aggregate with a dihedral angle approaching the dihedral angle of the ledge site (i.e., $\theta_{agg} = \theta_{sub}$), providing for a greater decrease in σ_{23} for a given volume of the aggregate.* Furthermore, the ledge site orientation will dictate the orientation of the growing phase.

If prenucleation aggegates comprise relatively small numbers of molecules, the topography of the relevant crystal planes *on a*

(26) The notation $(hkl)_{step} \cap (hkl)_{terrace}$ will be used herein to describe two planes defined by a dihedral angle, where the symbol "$\cap$" denotes an intersection. The intersection of these two planes defines a line associated with a crystallographic direction common to both planes; therefore, $(hkl)_{step} \cap (hkl)_{terrace} = [uvw]_{sub}$.

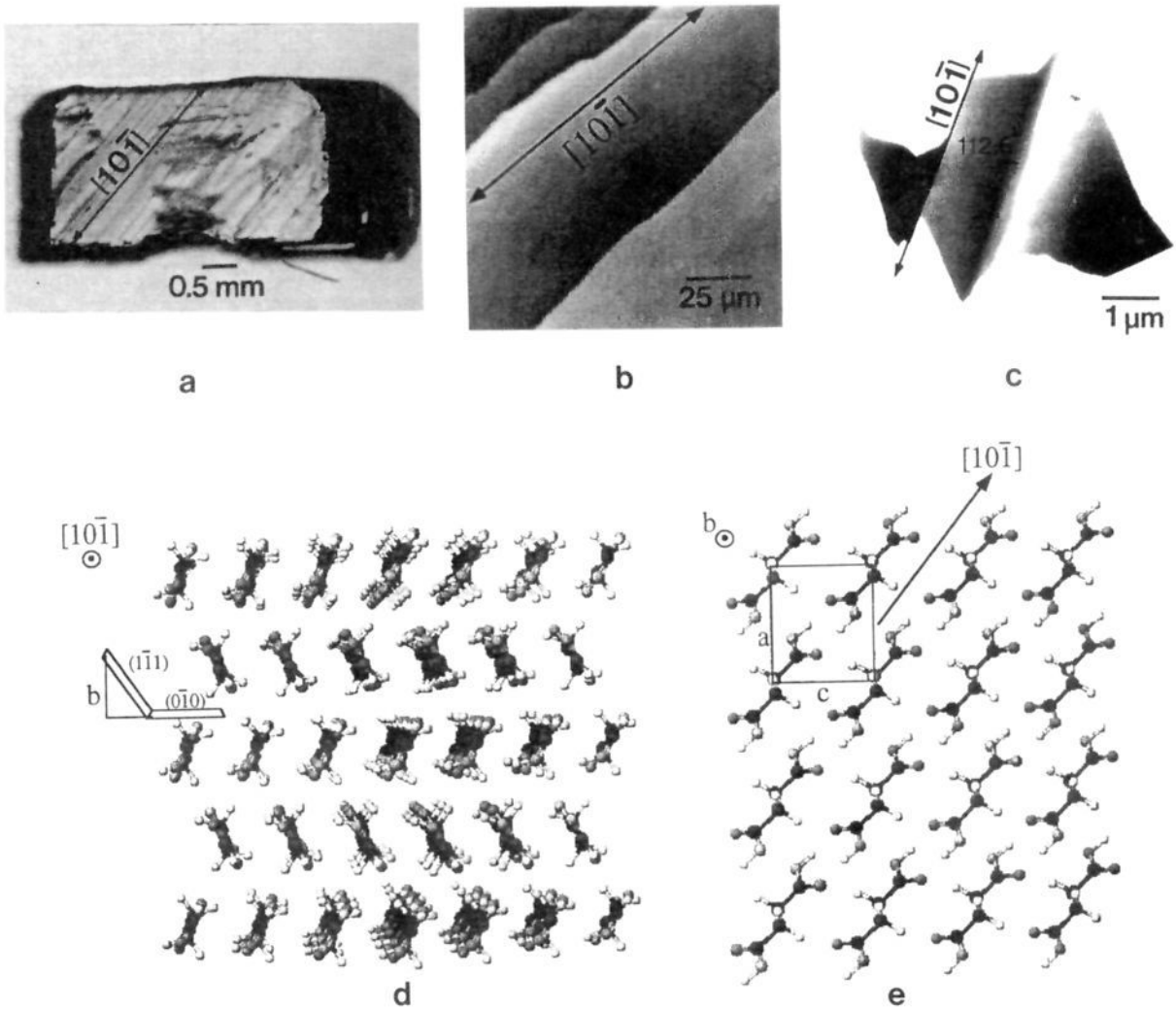

Figure 3. (a) A view of the $(0\bar{1}0)_{sa}$ face after cleaving solution grown crystals. The crystal was cleaved by applying pressure along the $[001]_{sa}$ direction with a sharp razor blade or microtome. Defects in the crystal were introduced by mechanical abrasion to compare crystal growth at these sites with growth at the naturally occurring ledges. (b) Phase measurement interferometric microscopy of the $(0\bar{1}0)_{sa}$ face and $[10\bar{1}]_{sa}$ ledges, which consist of $(0\bar{1}0)_{sa} \cap \{111\}_{sa}$. The terraces are indicated here as a contrast in gray scale, with step heights <80 nm. (c) Atomic force microscopy of the $(0\bar{1}0)_{sa}$ face and $[10\bar{1}]_{sa}$ ledges. The angle indicated was determined by line profile analyses of the AFM data. (d) Crystal structure of succinic acid. The $(0\bar{1}0)_{sa}$ and the $(1\bar{1}1)_{sa}$ are illustrated. (e) Molecular structure of the $(0\bar{1}0)_{sa}$ plane. The $[10\bar{1}]_{sa}$ ledges that persist on all length scales are a manifestation of strong hydrogen bonding along this direction.

nanometer length scale also can be a significant factor in nucleation. In crystallization from the gas phase, aggregates can form by coalescence of molecular species that have condensed on the substrate ledges (Figure 2b). Attractive van der Waals forces at the substrate–aggregate interface will rely on the *molecular* corrugation of the substrate and aggregate planes contacting the substrate during nucleation. These forces will be greatest when the topographies of corrugated substrate surfaces and aggregates are in perfect registry, or if the interfacial surfaces of the substrate and aggregate are molecularly flat on the scale of the aggregate size. Since the former condition would be highly fortuitous, nucleation will more commonly involve molecularly flat, densely packed crystal planes. These considerations, and comparison to simple epitaxy principles, are exemplified below.

Results

Crystal Growth Substrates. In order to examine the role of ledges and terraces in nucleation and growth, the substrates must have internal properties that favor the presence of well-defined terraces, step planes, and ledges on the substrate surfaces. These features will be favored if the substrate contains two or more planes that can form low-energy terraces and step planes, which in turn will be favored if crystal planes are available that are molecularly smooth and contain strong intermolecular interactions within the planes. Ledges containing these planes will be favored along a lattice direction, common to these two planes, corresponding to an axis containing the strong intermolecular interaction. The presence of strong intermolecular interactions also inhibits surface reconstruction, which is an important consideration when elucidating the relationship between nucleation behavior and surface topography. These criteria are satisfied by certain organic hydrogen bonded solids, including succinic acid and L-valine. The latter also was chosen as a substrate in order to examine the role of polar interactions in nucleation.

Succinic Acid Surface Structure. Succinic acid crystallizes in the monoclinic space group $P2_1/c$ (a = 5.519 Å, b = 8.862 Å, c = 5.101 Å, and β = 91.6°).[27] The crystal structure of succinic acid reveals hydrogen-bonded succinic acid chains arranged in sheets parallel to $\{010\}_{sa}$, with the chains oriented along the $[10\bar{1}]_{sa}$ direction (Figure 3). The conventional notation for crystallographic directions and planes is used here.[28] Each succinic acid molecule makes four hydrogen bonds manifested by O–H···O

(27) Leviel, J.-L.; Auvert, G.; Savariault, J.-M. *Acta Crystallogr.* **1981**, *B37*, 2185.

contacts of 2.64 Å between the carboxylic acid groups. Crystals of succinic acid grown in water are diamond-shaped plates with well-developed $\{100\}_{sa}$ faces and smaller $\{010\}_{sa}$, $\{111\}_{sa}$, and $\{001\}_{sa}$ faces, consistent with previous reports.[29] These single crystals can be cleaved readily by applying a small force with a sharp razor blade or microtome along $[001]_{sa}$ on the $(100)_{sa}$ face. This procedure provides freshly prepared, clean $\{010\}_{sa}$ surfaces, with typical dimensions of 3 mm × 9 mm.

The $\{010\}_{sa}$ faces of freshly cleaved succinic acid crystals possess linear features along $[10\bar{1}]_{sa}$ which are observed readily by optical microscopy (Figure 3a). Cleaving a succinic acid crystal actually produces both $(010)_{sa}$ and $(0\bar{1}0)_{sa}$ surfaces, which are mirror images of each other under the monoclinic lattice symmetry. Assignment of the linear features on the succinic acid crystal to $[10\bar{1}]_{sa}$ requires that the crystal plane viewed in Figure 3 be assigned as $(0\bar{1}0)_{sa}$ by convention (that is, the $[010]_{sa}$ direction projects away from the viewer). Subsequent discussions will describe results using this crystal orientation.

Phase measurement interferometric microscopy (PMIM) and atomic force microscopy (AFM) indicated that the features along $[10\bar{1}]_{sa}$ were macroscopic ledges with heights ranging from 5 to >500 nm. A typical PMIM image of the $(0\bar{1}0)_{sa}$ face revealed steps running parallel to $[10\bar{1}]_{sa}$, with the surface profile indicating flat $(0\bar{1}0)_{sa}$ terraces (Figure 3b). Atomic force microscopy of the $(0\bar{1}0)_{sa}$ surface also revealed steps along $[10\bar{1}]_{sa}$ (Figure 3c). The crystallographic identity of the step plane separating the $(0\bar{1}0)_{sa}$ terraces could not be identified by PMIM due to insufficient in-plane spatial resolution (0.77 μm). However, AFM experiments indicated that the minimum dihedral angle between $(0\bar{1}0)_{sa}$ terraces and the step planes was 113°, which is greater than the reported minimum resolvable angle for these tips (105°).[30] The agreement of this value with the $(0\bar{1}0)_{sa} \cap \{111\}_{sa}$[26] dihedral angle determined from the crystal structure (112.6°), combined with the requirement that the step plane must contain $[10\bar{1}]_{sa}$, strongly favors assignment of the step plane as $(111)_{sa}$ or $(1\bar{1}1)_{sa}$.

Both the $\{010\}_{sa}$ and $\{111\}_{sa}$ crystallographic planes have high molecular packing densities and comprise layers of hydrogen-bonded chains. These planes can be characterized as low-energy surfaces as there is strong hydrogen bonding between succinic acid molecules *parallel* to these planes and minimal molecular corrugation. Strong hydrogen bonding along the succinic acid chains parallel to $[10\bar{1}]_{sa}$ favors cleavage along planes containing this direction. Weak van der Waals forces between $\{010\}_{sa}$ and $\{111\}_{sa}$ layers are responsible for the predominance of the $\{010\}_{sa}$ and $\{111\}_{sa}$ planes in the cleaved crystal. *The structure and microscopy results therefore support a surface topography principally consisting of* $[10\bar{1}]_{sa}$ *ledges containing the* $(0\bar{1}0)_{sa} \cap \{111\}_{sa}$ *planes.* We note that numerous reports describing STM and AFM of low-energy planes of organic crystals indicate that reconstruction of their exposed surface planes is not common.[31] Indeed, the only reported example of surface reconstruction is the (001) face of pyrene, which has only van der Waals forces between molecules parallel to the (001) plane.[32] It is reasonable to suggest that the strong hydrogen bonding parallel to the ledge planes on the succinic acid substrate will inhibit surface reconstruction of the ledge site; therefore, the molecular structure of the crystal planes and the structure of the ledge can be deduced from the crystal structure.

L-Valine Surface Structure. L-Valine crystallizes in the monoclinic space group $P2_1$ (a = 9.71 Å, b = 5.27 Å, c = 12.06 Å, and β = 90.8°).[33] The crystal structure of L-valine reveals $(001)_{val}$ layers containing L-valine molecules related by translation symmetry. The L-valine molecules within the layer are held together by van der Waals contacts between the isopropyl groups and hydrogen bonding with NH···O contacts of 2.78 and 2.86 Å (Figure 4). While the individual layers are assembled in bilayers by further hydrogen-bonding interactions between the layers, the bilayers are separated from each other by weak van der Waals contacts between isopropyl groups. This suggests that the $(001)_{val}$ faces generated by cleavage will have isopropyl groups exposed at the surface, consistent with contact angle measurements with water which indicate that these surfaces are hydrophobic.[19] Individual bilayers are held together by two-dimensional hydrogen bonding within the $(001)_{val}$ sheet, in contrast to the highly one-dimensional hydrogen bonding in $(010)_{suc}$. As a consequence of the two-dimensional hydrogen-bonding network, L-valine crystals grown in water are diamond-shaped plates with well-developed $(001)_{val}$ faces elongated along the a axis. The $(110)_{val}$, $(\bar{1}10)_{val}$, $(1\bar{1}0)_{val}$, and $(\bar{1}\bar{1}0)_{val}$ planes are also prominent. Cleaving these crystals with a razor blade or microtome along $[100]_{val}$ results in the formation of *fresh* large $(001)_{val}$ faces with typical surface areas around 30 mm^2. The $(001)_{val}$ surface possesses ledges predominantly oriented along the $[010]_{val}$ direction. PMIM indicates that the average ledge height on the $(001)_{val}$ face is <150 nm, smaller than the ledge heights on $(0\bar{1}0)_{sa}$ (Figure 4b). Further inspection of the crystal structure of L-valine reveals that the $(\bar{2}01)_{val}$ plane, which contains $[010]_{val}$, has high molecular packing density and small molecular corrugation. Indeed, AFM experiments revealed surface features with dihedral angles of 111.2°, in agreement with the $(\bar{2}01)_{val} \cap (001)_{val}$ dihedral angle determined from the crystal structure. Macroscopic curvature of the ledges is evident in some regions. Based on the morphology of solution grown crystals and inspection of the crystal structure, it is reasonable to assign this behavior to the presence of $\{110\}_{val}$ and $\{\bar{1}10\}_{val}$ planes, which would form $[\bar{1}10]_{val}$ and $[110]_{val}$ ledges, respectively. It is therefore likely that the curved ledges result from kinks comprising $[010]_{val}$ and $[\bar{1}10]_{val}$ (or $[110]_{val}$).

Nucleation and Growth. Crystallization of benzoic acid on a freshly cleaved succinic acid crystal substrate at sublimation temperatures between 35 and 60 °C produced *oriented* single crystals of benzoic acid crystals on the $(0\bar{1}0)_{sa}$ face growing from the $[10\bar{1}]_{sa}$ ledges, with nucleation frequencies approaching 50 mm^{-2} (Figure 5).[34] At these temperatures the partial pressure

(28) The notation used here is the conventionally accepted one, in which {*hkl*} refers to a family of crystallographically equivalent planes or faces, (*hkl*) refers to a specific crystal plane, and [*uvw*] refers to a specific direction. Therefore, when describing behavior that pertains to all equivalent planes in a family, the {*hkl*} notation will be used. When describing behavior that pertains to only one plane in that family, the specific (*hkl*) plane is noted.

(29) (a) van der Voort, E. *J. Cryst. Growth* **1991**, *110*, 662. (b) Davey, R. J.; Mullin, J.W.; Whiting, M. J. L. *J. Cryst. Growth* **1982**, *58*, 304.

(30) It is important to note that AFM can accurately measure dihedral angles only for large steps (>150 nm) where the area of the tip contacting the step does not change with translation across the step. For steps with small heights, or steps with dihedral angles approaching 90°, the tip contact point changes with translation and results need to account for tip geometries. The radius of curvature of the tip influences topographical mapping of all small steps and step edges, but dihedral angles between planes with large surface areas can be determined independent of tip geometry. The maximum attainable resolution of the dihedral angle using "normal" AFM tips is limited by the tip geometry to angles ≥129° due to lateral forces encountered at a step for a tip with an aspect ratio less than the inclined step plane. The 129° angle is experimentally observed as the smallest dihedral angle measured between the step and $(0\bar{1}0)_{sa}$ surface using these tips instead of the ultralever tips described in the Experimental Section.

(31) (a) Gould, S.; Marti, O.; Drake, B.; Hellemans, L.; Bracker, C. E.; Hansma, P. K.; Keder, N. L.; Eddy, M. M.; Stucky, G. D. *Nature* **1988**, *332*, 332. (b) Overney, R. M.; Howald, L.; Frommer, J.; Meyer, E.; Guntherodt, H.-J. *J. Chem. Phys.* **1991**, *94*, 8441. (c) Fainchtein, R.; Murphy, J. C. *J. Vac. Sci. Technol. B* **1991**, *9*, 1013. (d) Pan, S.; Delozanne, A. L.; Fainchtein, R. *J. Vac. Sci. Technol. B* **1991**, *9*, 1017–1021. (e) Sleator, T.; Tycko, R. *Phys. Rev. Lett.* **1988**, *60*, 1418. (f) Magonov, S. N.; Schuchhardt, J.; Kempf, S.; Keller, E.; Cantow, H.-J. *Synth. Met.* **1991**, *40*, 59–72. (g) Magonov, S. N.; Kempf, S.; Rotter, H.; Cantow, H.-J. *Synth. Met.* **1991**, *40*, 73–86. (h) Li, S.; White, H. S.; Ward, M. D. *Chem. Mater.* **1992**, *4*, 1082. (i) Li, S.; White, H. S.; Ward, M. D. *J. Phys. Chem.* **1992**, *96*, 9014.

(32) Overney, R. M.; Howald, L.; Frommer, J.; Meyer, E.; Brodbeck, D.; Guntherodt, H.-J. *Ultramicroscopy* **1992**,*42*, 983.

(33) Torii, K.; Iitaka, Y. *Acta. Crystallogr.* **1970**, *B26*, 1317.

(34) We note that the distribution of symmetry equivalent (111) and $(1\bar{1}1)$ steps is likely to vary for each $(010)_{suc}$ surface. In some cases, benzoic acid growth at ledge sites with $(010)_{sa} \cap (111)_{sa}$ planes could be distinguished from growth at ledges with $(010)_{sa} \cap (1\bar{1}1)_{sa}$ planes. However, growth from either ledge results in the same orientation, and PMIM measurements indicate that when the ledge height is <100 nm the needle-like benzoic acid crystals grow over the ledge sites. These factors make it difficult to establish whether growth was initiated from $(111)_{sa}$ or $(1\bar{1}1)_{sa}$ step planes in all cases.

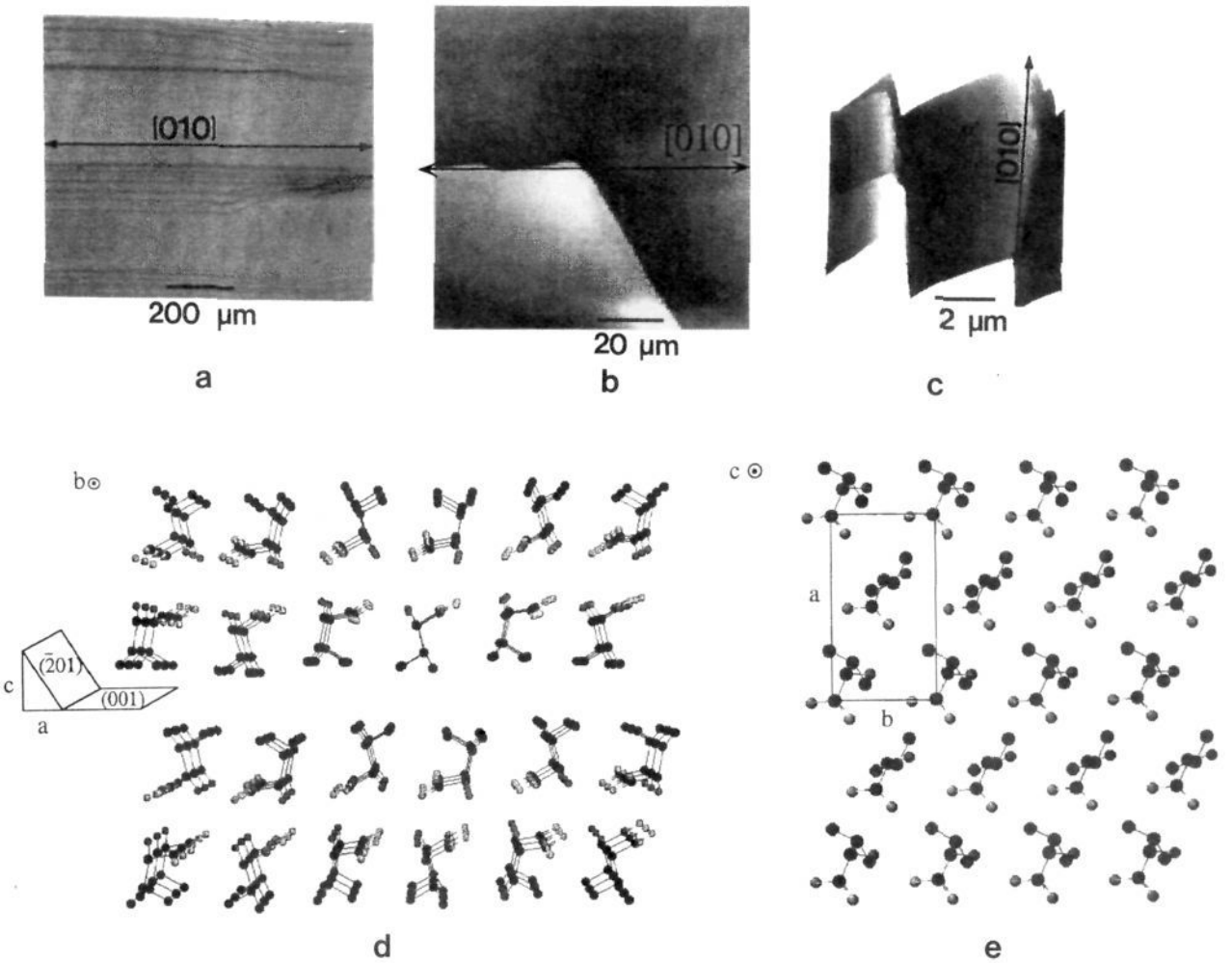

Figure 4. (a) A view of the $(001)_{val}$ face after cleaving solution grown crystals. The crystal was cleaved by applying pressure parallel to the (001) face with a sharp razor blade or microtome. (b) Surface profile of the $(001)_{val}$ face and the $[010]_{val}$ ledge site containing the $(001)_{val} \cap (\bar{2}01)_{val}$ planes obtained with phase measurement interferometric microscopy. (c) Atomic force microscopy of the $(001)_{val}$ face and the $[010]_{val}$ ledge site containing the $(001)_{val} \cap (\bar{2}01)_{val}$ planes. The angle indicated was determined by line profile analyses of the AFM data. (d) Crystal structure of L-valine. The $(001)_{val}$ and the $(\bar{2}01)_{val}$ planes are illustrated. (e) Molecular structure of the $(001)_{val}$ plane. Hydrogen atoms have been omitted for clarity.

of benzoic acid ranges from 3 to 35 mTorr while the vapor pressures of the substrate crystals were 1–3 orders of magnitude less.[35] Crystallographic analysis revealed that the benzoic acid crystallized in the monoclinic space group $P2_1/c$ (a = 5.52 Å, b = 5.14 Å, c = 21.9 Å, and β = 97°). This is identical to the common previously reported phase,[36] in which benzoic acid molecules form dimers that are assembled into stacks, the stacks in turn assembled into sheets parallel to the $(001)_{ba}$ plane (Figure 6). Crystallographic analysis also indicated that the crystals predominantly were oriented as "*A*" (>80%) such that the $(001)_{ba}$ plane was in contact with $(0\bar{1}0)_{sa}$, with the $[010]_{ba}$ axis oriented at an angle of 46° ± 1.7° with respect to $[10\bar{1}]_{sa}$. The $[100]_{sa}$ makes a 42° angle with $[10\bar{1}]_{sa}$; therefore, $[010]_{ba}$ is *not* coincident with $[100]_{sa}$. As the supersaturation was lowered, the nucleation frequency decreased and the preference for orientation *A* increased. Furthermore, inspection of the grown crystals reveals that orientation *B* results from nucleation at existing crystals in orientation *A*, *not* from nucleation at succinic acid ledge sites.

The behavior observed for crystallization of 4-nitroaniline is similar to that observed for benzoic acid in many respects, as exhibited by the formation of oriented, rectangular single crystals of 4-nitroaniline at the $[10\bar{1}]_{sa}$ ledges (Figure 5). The crystals belonged to the centrosymmetric monoclinic space group $P2_1/n$ (a = 12.34 Å, b = 6.07 Å, c = 8.59 Å, and β = 91.45°), identical to the only known phase of 4-nitroaniline.[37] The solid-state structure of this compound contains hydrogen-bonded chains along the $[10\bar{1}]_{pna}$ axis which are arranged head to tail by hydrogen bonding between nitro and amine groups (O–N contact distances of 3.07 Å), with the chains assembled into densely packed, polar $(101)_{pna}$ layers (Figure 7). Large $(101)_{pna}$ faces contacted $(0\bar{1}0)_{sa}$, and $[10\bar{1}]_{pna}$ was aligned with $[10\bar{1}]_{sa}$. Under mild saturation conditions (nucleation frequencies between 100 and 1000 mm^{-2}) 4-nitroaniline crystals grew *exclusively* on the $[10\bar{1}]_{sa}$ ledges.

Crystal growth on L-valine substrates resembled the behavior observed on succinic acid. Benzoic acid crystals grew on $(001)_{val}$ at very low driving forces with a habit similar to that observed on $(0\bar{1}0)_{sa}$ (Figure 8). In this case the $(001)_{ba}$ crystallographic plane formed an interface with $(001)_{val}$, and $[010]_{ba}$ was coincident with $[010]_{val}$. Benzoic acid crystal growth clearly was initiated at ledge sites present on the substrate. Growth of benzoic acid crystals over ledges was more evident than on succinic acid, which is attributed to the smaller ledge heights on L-valine. Similarly, crystals of the $P2_1/n$ phase of 4-nitroaniline formed at $[010]_{val}$ ledge sites, with $(101)_{pna}$ contacting $(001)_{val}$. Crystallographic analysis and assignment of orientation based on well-understood morphological features indicated that >90% of the

(35) (a) Davies, M.; Jones, J. I. *Trans. Faraday Soc.* **1954**, 1042. (b) Davies, M.; Thomas, G. H. *Trans Faraday Soc.* **1960**, *56*, 185.

(36) Sim, G. A.; Robertson, J. M.; Goodwin, T. H. *Acta Crystallogr.* **1955**, *8*, 157.

(37) Trueblood, K. N.; Goldish, E.; Donahue, J. *Acta. Crystallogr.* **1961**, *14*, 1009.

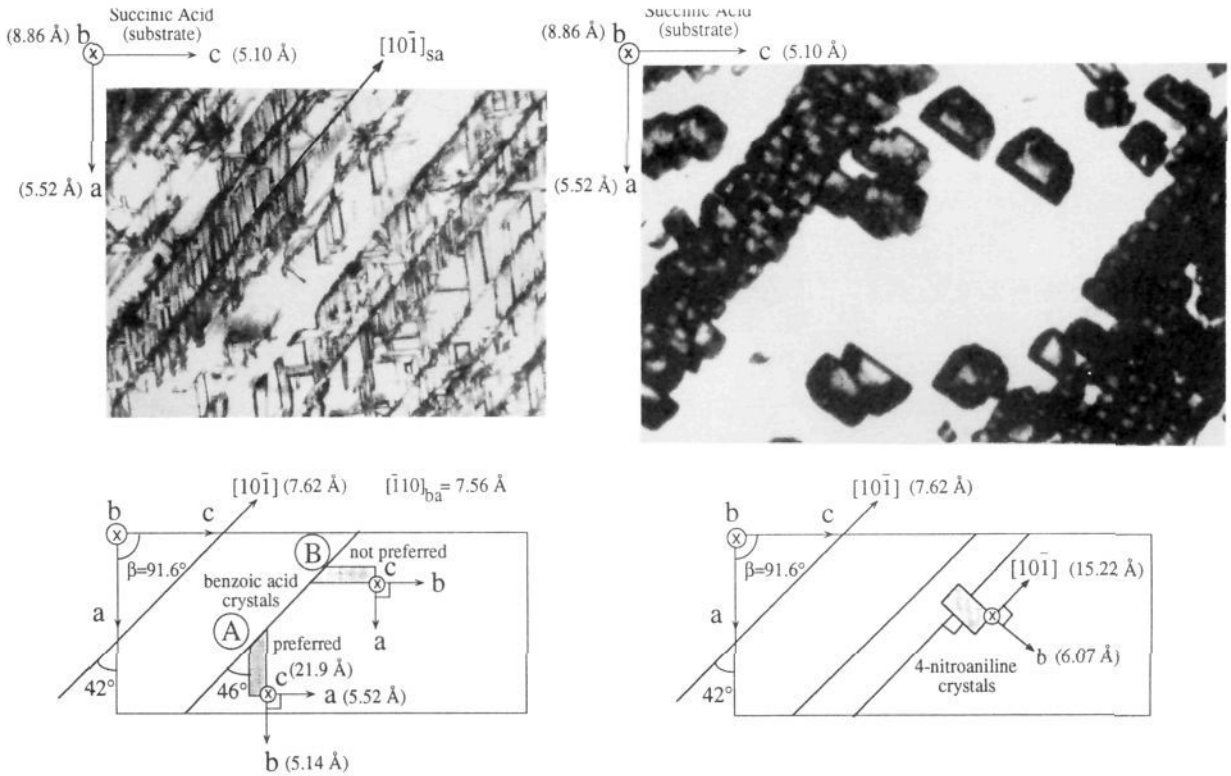

Figure 5. (a) Top, oriented benzoic acid crystals grown from the gas phase onto $(0\bar{1}0)_{sa}$. Bottom, schematic representation of the orientations of benzoic acid on $(0\bar{1}0)_{sa}$. The preferred orientation represents >80% of the mature crystals and almost 100% of the benzoic acid crystals initiated from $[10\bar{1}]_{sa}$ ledges. The lattice parameters and directions for succinic acid and benzoic acid are also depicted. (b) Top, oriented 4-nitroaniline crystals grown from the gas phase onto $(0\bar{1}0)_{sa}$. Bottom, schematic representation of the preferred orientation and lattice parameters of 4-nitroaniline on $(0\bar{1}0)_{sa}$.

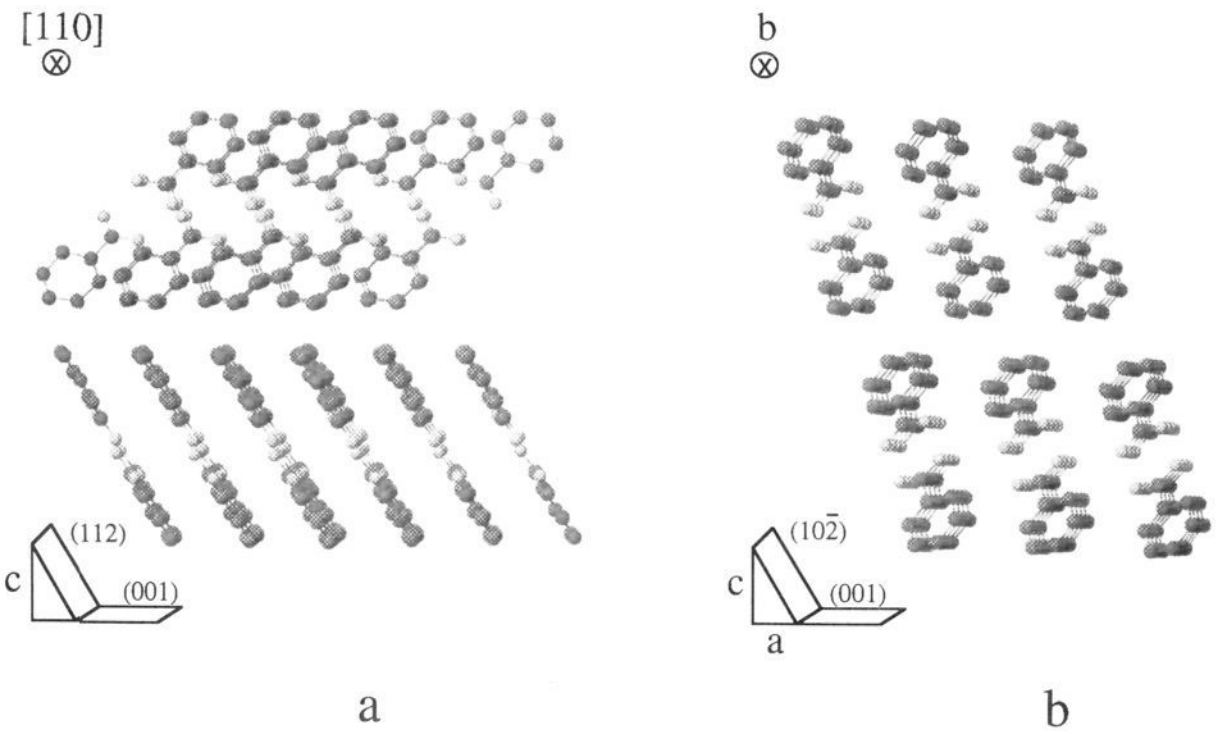

Figure 6. (a) Crystal structure of benzoic acid illustrating the $(001)_{ba}$ and $(112)_{ba}$ planes. (b) Crystal structure of benzoic acid illustrating the $(001)_{ba}$ *and* $(10\bar{2})_{ba}$ *planes. Hydrogen atoms have been omitted for clarity.*

crystals were oriented with $[10\bar{1}]_{pna}$ (the chain axis direction) parallel to $[010]_{val}$ (Figure 8). In the case of 4-nitroaniline, a small number of crystal growth events were occasionally observed on regions of the L-valine substrate in which steps were not present. In these cases, crystal orientations tended to be random, illustrating the importance of the ledge in directing growth.

Under the conditions examined, benzoic acid and 4-nitroaniline nucleation occurred *exclusively* on the succinic acid and L-valine

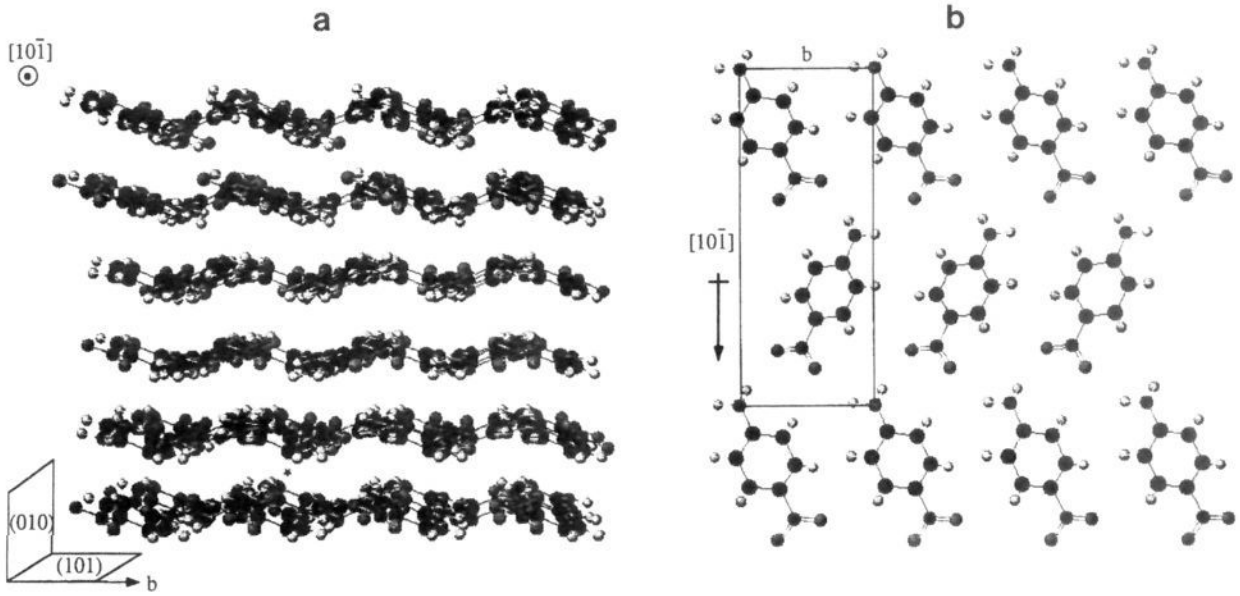

Figure 7. (a) The crystal structure of 4-nitroaniline viewed parallel to the $(101)_{pna}$ hydrogen-bonded layers. One of the inversion centers between $(101)_{pna}$ layers is indicated by the asterisk. (b) Top view of a $(101)_{pna}$ layer. The arrow indicates the orientation of the layer dipole, which is coincident with the $[10\bar{1}]_{pna}$ direction. The length of $[10\bar{1}]_{pna}$ = 15.22 Å.

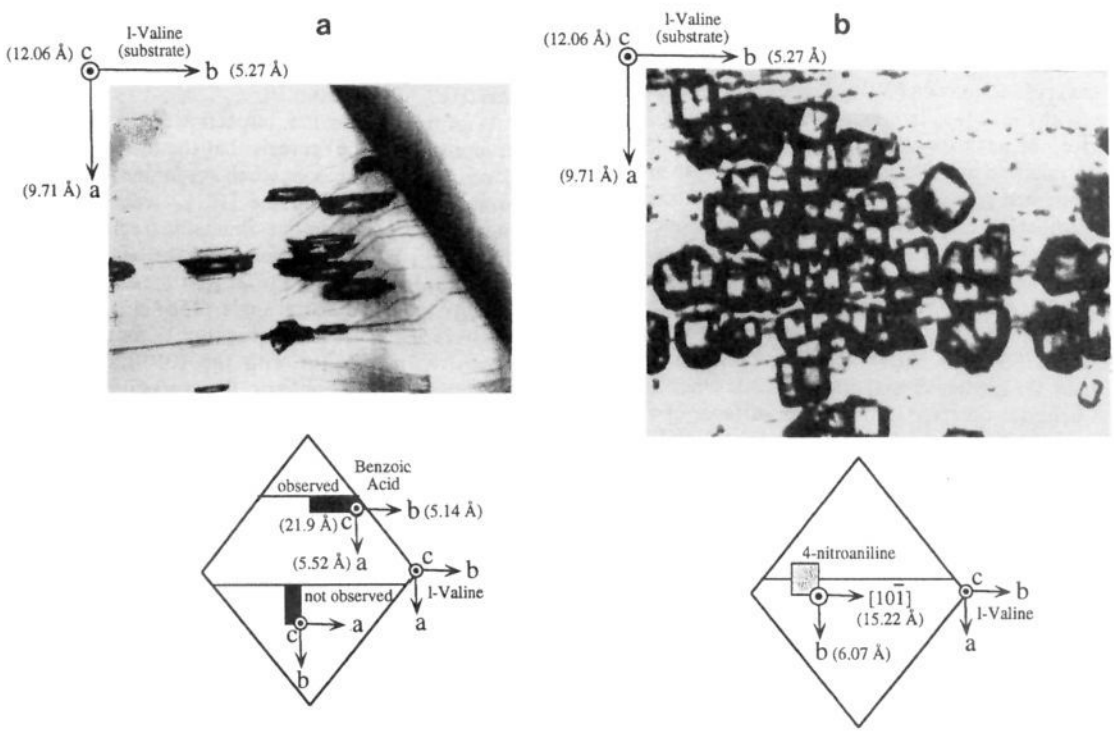

Figure 8. (a) Top: oriented benzoic acid crystals grown on $(001)_{val}$ with a schematic of the observed relative orientations below. (b) Top: oriented 4-nitroaniline crystals grown on $(001)_{val}$ with a schematic of the observed orientations shown below.

substrates, and not on other glass surfaces within the sublimation apparatus. Nucleation also was absent on substrate defects that occurred naturally or were purposely introduced by mechanical abrasion. Crystal growth was observed on walls of the sublimation apparatus and areas of the substrate other than the $[10\bar{1}]_{sa}$ or $[010]_{val}$ ledges only when sublimation temperatures exceeded 60 °C, at which the substrates were decorated with randomly oriented clusters of benzoic acid needles. Randomly oriented growth also was observed on glass or mica substrates, with nucleation occurring at higher driving forces than that required on succinic acid or L-valine.

In order to examine nucleation on more polar molecular crystal substrates, we examined nucleation on malonic acid and α-glycine. α-Glycine crystallizes in the monoclinic space group $P2_1/n$ (a = 5.102 Å, b = 11.971 Å, c = 5.457 Å, and β = 111.7°).[38] The crystals are bipyramidal with well-developed $(110)_{gly}$ and $(011)_{gly}$ faces capped by $(010)_{gly}$ and $(0\bar{1}0)_{gly}$ faces, in agreement with previous reports.[39] Cleaving α-glycine crystals with a razor blade along $[001]_{gly}$ produces large $(010)_{gly}$ faces with surface areas of 30–50 mm^2. The $(010)_{gly}$ surface produced by cleaving has ledges parallel to $[100]_{gly}$ and $[001]_{gly}$ with heights ranging from 10 to 1000 nm, as measured by PMIM and AFM. As in the case of

(38) (a) Albrecht, G.; Corey, R. B. *J. Am. Chem. Soc.* **1939**, *61*, 1087. (b) Power, L. F.; Turner, K. E.; Moore, F. H. *Acta Crystallogr.* **1976**, *B32*, 11.

(39) Weissbuch, I.; Addadi, L.; Berkovitch-Yellin, Z.; Gati, E.; Weinstein, S.; Lahav, M.; Leiserowitz, L. *J. Am. Chem. Soc.* **1983**, *105*, 6615.

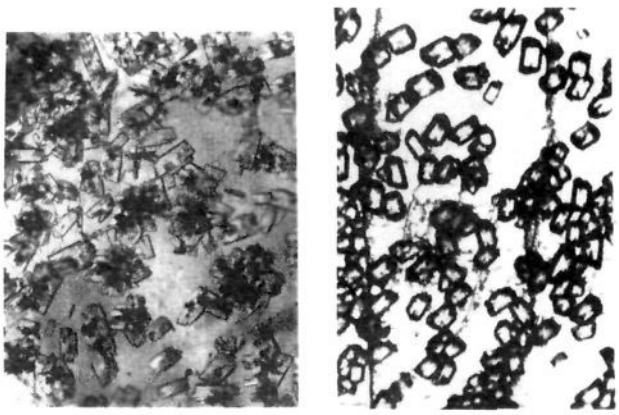

Figure 9. (a) Randomly oriented benzoic acid crystals grown on the (010) face of glycine. (b) Randomly oriented of 4-nitroaniline crystals grown on the (100) face of malonic acid.

succinic acid, strong hydrogen bonding along $[100]_{gly}$ (N–H···O = 2.88 Å) and $[001]_{gly}$ (N–H···O = 2.76 Å) is responsible for these topographic features. Weak van der Waals interactions are present between bilayer sheets contained in the $(010)_{gly}$ planes. Based on the morphology of solution grown α-glycine crystals, the $[100]_{gly}$ and $[001]_{gly}$ ledges most likely contain $(011)_{gly} \cap (010)_{gly}$ and $(110)_{gly} \cap (010)_{gly}$, respectively.

At temperatures approaching 40 °C, rectangular prisms of benzoic acid crystals grew on $(010)_{gly}$, preferentially at step and ledge sites, with the $(001)_{ba}$ interface contacting $(010)_{gly}$ (Figure 9). However, the nucleation frequency was significantly lower than on succinic acid and the crystals were *randomly* oriented. Randomly oriented growth of 4-nitroaniline also is observed on $(010)_{gly}$. Furthermore, crystallization of 4-nitroaniline on the $(100)_{mal}$ plane of malonic acid, a plane containing hydrogen-bonded chains that can be exposed by cleaving solution grown diamond-shaped crystals, results in randomly oriented crystals (malonic acid crystallizes in the triclinic $P\bar{1}$ space group; a = 5.37 Å, b = 5.16 Å, c = 11.35 Å, α = 102.7°, β = 135.4°, γ = 85.0°). In all these cases, the random crystal orientations are indistinguishable from behavior observed on the polar surfaces of glass or mica. The nucleation frequencies are also much smaller than those observed on succinic acid and L-valine. While this collection of substrates is rather limited at the present time, the results suggest that nucleation and orientation are much less predominant on more polar surfaces (*vide infra*).

Discussion

The nucleation and growth of benzoic acid and 4-nitroaniline on succinic acid and L-valine clearly indicate that well-defined ledges on these substrates are effective in promoting nucleation and oriented growth at low driving forces. Particularly noteworthy is the orientation of benzoic acid crystals on succinic acid. The lattice constants of the two unit cell axes contained in the $(0\bar{1}0)_{sa}$ terrace (a = 5.52 Å, c = 5.10 Å) are nearly identical to those contained in the $(001)_{ba}$ plane (a = 5.52 Å, b = 5.14 Å), yet $[001]_{ba}$ is aligned with $[001]_{sa}$, and $[010]_{ba}$ is nearly aligned with $[100]_{sa}$. *This is contrary to expectation based on a simple two-dimensional (or even one-dimensional) epitaxy model based on the unit cell constants*, as there exists an exact one-dimensional lattice match of $[100]_{ba}$ and $[100]_{sa}$ directions and only a small 0.8% mismatch between the $[010]_{ba}$ and $[001]_{sa}$ directions (Figure 5). Nucleation driven by two-dimensional epitaxy is probably unfavorable due to the 1.7° difference between β_{sa} and γ_{ba}, the angles between the unit cell axes contained in the $(0\bar{1}0)_{sa}$ and the $(001)_{ba}$ planes, respectively. This small angular difference may be sufficient to disrupt favorable epitaxy between aggregate and substrate. The forces between contacting planar surfaces have been shown by others to be strongly dependent on their relative orientation.[40] Rather than simple two-dimensional nucleation on the substrate terraces, nucleation was initiated from the $[10\bar{1}]_{sa}$ ledges.

The angle between the $[010]_{ba}$ and $[110]_{ba}$ (or $[1\bar{1}0]_{ba}$) directions is 47°, in agreement with the angle between the $[010]_{ba}$ direction of the oriented benzoic acid crystals and $[10\bar{1}]_{sa}$ on the succinic acid substrate (the $[110]_{ba}$ and $[1\bar{1}0]_{ba}$ are crystallographically identical, but we will restrict the discussion to the $[110]_{ba}$ axis for simplicity). This strongly supports a nucleation mechanism involving an interface in which $[10\bar{1}]_{sa}$ and $[110]_{ba}$ are coincident. Indeed, an epitaxial lattice match between $[10\bar{1}]_{sa}$ and $[110]_{ba}$ is suggested by their scalar magnitudes of 7.62 and 7.54 Å, respectively. This 1.04% lattice mismatch is small enough to expect stabilization and orientation of prenucleation aggregates.[41] However, the observation that growth occurs predominantly on $[10\bar{1}]_{sa}$ *ledges*, and not on ledge-free regions, indicates that nucleation *must involve both planes of the ledge*. Nucleation solely from $\{111\}_{sa}$ is not consistent with the observed orientation effects, which result from interaction between $(0\bar{1}0)_{sa}$ and $(001)_{ba}$. These results indicate that two planes of the prenucleation aggregate (which are presumed to correspond to the planes in the mature crystal) interact with both planes of the ledge, the aggregate planes sharing the $[110]_{ba}$ direction and having a dihedral angle near that of the ledge site. The interfacial interactions at the ledge site would be strongest between planes with minimum repulsive interactions and molecularly flat surfaces that can maximize dispersive forces at the interface.

With these guidelines, inspection of the benzoic acid crystal structure (Figure 6) reveals that the $(001)_{ba} \cap \{112\}_{ba}$ pair of planes is the most reasonable choice for the interface between the putative aggregate and the $[10\bar{1}]_{sa}$ ledge (Figure 10). This interface maintains the one-dimensional epitaxy between $[110]_{ba}$ and $[10\bar{1}]_{sa}$ lattice directions, and the benzoic acid $(001)_{ba} \cap \{112\}_{ba}$ dihedral angle of 113.2° is within 0.6° of the succinic acid $(0\bar{1}0)_{sa} \cap \{111\}_{sa}$ dihedral angle. The $(112)_{ba}$ and $(001)_{ba}$ planes also have low molecular corrugation that can result in favorable dispersive interactions with the $(0\bar{1}0)_{sa}$ and $\{111\}_{sa}$ planes, respectively. This geometrically favored interfacial stabilization of the aggregate with both planes of the ledge site can be described as "ledge directed epitaxy". Further analysis of the benzoic acid crystal structure reveals that participation of other interfaces in nucleation is unlikely on the basis of dihedral angle, molecular roughness of the planes and the requirement that the ledge site contain $[10\bar{1}]_{sa}$ (tables comparing the length and dihedral angles of the substrate and nucleant planes are available in the supplementary material).

If only the ledge direction and dihedral angle are considered in ledge directed epitaxies, orientations A and B in Figure 5 are equally likely, as orientation B also allows an epitaxial match of $[110]_{ba}$ with $[10\bar{1}]_{sa}$ and a dihedral angle match between substrate and aggregate planes. The observed orientation preference must be a consequence of the monoclinic symmetry of the substrate, which renders these two orientations crystallographically, and therefore chemically, different. Orientation B is related to orientation A by symmetry operations not allowed by the monoclinic lattice (e.g., a 2-fold rotation about $[101]_{sa}$). While inspection of the crystal structure and the relevant faces does not reveal any obvious chemical origins for the orientation preference, the crystallographic inequivalence of these directions mandates that these orientations have different energies.

In the case of benzoic acid nucleation on L-valine, the angles between the unit cell axes contained in the contacting interfaces of the substrate and benzoic acid are identical (α = 90° for $[100]_{val}$

(40) McGuiggan, P. M.; Israelachvili, J. N. *Mater. Res. Soc. Symp. Proc.* **1989**, *138*, 349.

(41) Kasukabe, Y.; Osaka, T. *Thin Solid Films* **1987**, *146*, 175.

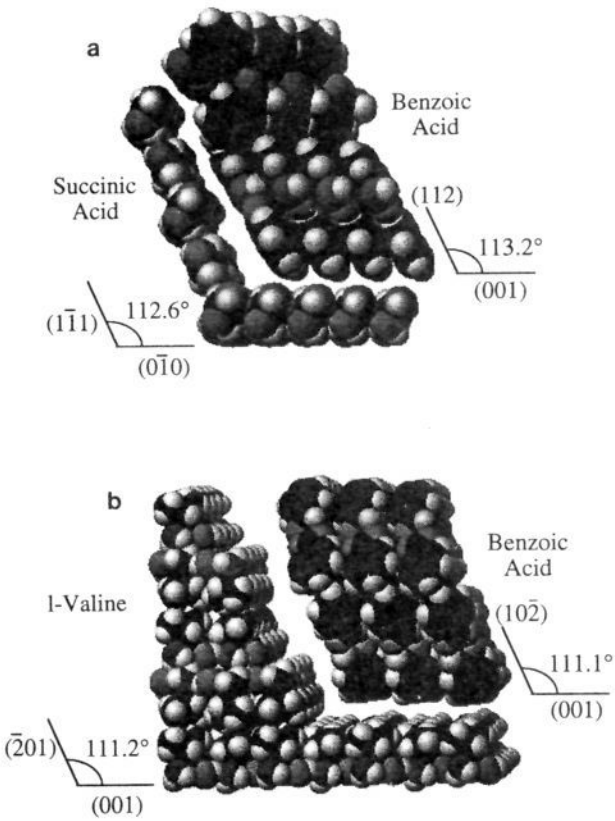

Figure 10. (a) Space-filling representation of a benzoic acid prenucleation aggregate and a succinic acid $[10\bar{1}]_{pna}$ ledge site containing the $(0\bar{1}0)_{sa} \cap (1\bar{1}1)_{sa}$ planes, illustrating the dihedral angle match with the contacting pair of $(001)_{ba} \cap (112)_{ba}$ planes of the aggregate. (b) Space-filling representation of a benzoic acid prenucleation aggregate and a $[010]_{val}$ ledge site containing the $(001)_{val} \cap (\bar{2}01)_{val}$ planes, illustrating the dihedral angle match with the contacting pair of $(001)_{ba} \cap (10\bar{2})_{ba}$ planes of the aggregate.

$\cap [010]_{val}$ and $[100]_{ba} \cap [010]_{ba}$). Therefore, the unit cell axes of the substrate and benzoic acid are aligned, in contrast to benzoic acid crystallization on succinic acid. However, comparison of L-valine and benzoic acid lattice parameters indicates lattice mismatches of 13.7% and 2.47% for $[100]_{val}$–$[100]_{ba}$ and $[010]_{val}$–$[010]_{ba}$, respectively. The orthogonal orientation at the interface, achieved by rotating $(001)_{ba}$ 90°, results in lattice mismatches of 4.74% and 5.87%, for $[100]_{val}$–$[010]_{ba}$ and $[010]_{val}$–$[100]_{ba}$, respectively. Therefore, a nucleation process driven by two-dimensional epitaxy is unlikely. Rather, based on the small lattice mismatch between $[010]_{val}$ and $[010]_{ba}$ and the observation of nucleation on pure $[010]_{val}$ ledge sites, it seems likely that the nucleation interface contains $[010]_{val}$ and $[010]_{ba}$. Notably, the dihedral angle of the $(10\bar{2})_{ba} \cap (001)_{ba}$ planes, which share the $[010]_{ba}$ axis, is 111.1°, nearly identical to the dihedral angle of the $[010]_{val}$ ledge determined by AFM. Although the $[101]_{val}$ ledge may also consist of $(201)_{val} \cap (001)_{val}$, its dihedral angle of 112.6° is 1.5° greater that the dihedral angle of $(10\bar{2})_{ba} \cap (001)_{ba}$. The molecular corrugation of $(201)_{val}$ also is larger than that of $(\bar{2}01)_{val}$. This suggests that the $(\bar{2}01)_{val}$ surface is more likely to prevail upon cleaving, and furthermore, would provide greater interfacial stabilization of the prenucleation aggregate. Therefore, we conclude that the $(\bar{2}01)_{val} \cap (001)_{val}$–$(10\bar{2})_{ba} \cap (001)_{ba}$ interface (Figure 10) is the most reasonable source of the observed nucleation.

The importance of ledges in nucleation was also evident in the crystallization of 4-nitroaniline. The $(101)_{pna}$ plane in contact with $(0\bar{1}0)_{sa}$ is relatively flat, although a slight puckering of the plane results from the hydrogen-bonding conformations. The $[010]_{pna}$ and $[10\bar{1}]_{pna}$ directions contained in the $(101)_{pna}$ are orthogonal to each other, while the angle between the unit cell axes contained in $(010)_{sa}$ is 91.6°. Therefore, an angular mismatch of 1.6° exists between these primary axes at the $(101)_{pna}$–$(0\bar{1}0)_{sa}$ interface. In addition, the $[010]_{pna}$ and $[101]_{sa}$ lattice parameters are 6.07 and 7.41 Å, respectively, indicating a rather poor lattice match between these directions. The absence of two-dimensional nucleation on $(0\bar{1}0)_{sa}$ is therefore not surprising.

A survey of the dihedral angles of 4-nitroaniline planes that share $[10\bar{1}]_{pna}$ reveals that the $(101)_{pna} \cap (121)_{pna}$ planes have the best dihedral match with the $[10\bar{1}]_{sa}$ ledge, with a difference of only 0.9°. The observation of nucleation only at the ledge sites is consistent with participation of both substrate planes. Fewer dispersive intermolecular contacts are expected at the $\{111\}_{sa} \cap (121)_{pna}$ interface because of the greater corrugation of the $(121)_{pna}$ that results from the "zigzag" motif in the 4-nitroaniline chains. However, this may be compensated by the formation of $[10\bar{1}]_{pna}$ 4-nitroaniline chains, which must be parallel to $[10\bar{1}]_{sa}$ in the observed orientation. The ΔG of these chains can be lowered by a favorable one-dimensional lattice epitaxy along the ledge (0.1% lattice mismatch between $[10\bar{1}]_{pna}$ (15.22 Å) and $[10\bar{1}]_{sa}$ (2 × 7.62 Å). In addition to dispersive interactions, hydrogen bonding between the free N–H of 4-nitroaniline and carbonyl oxygen atoms on the $(111)_{sa}$ step plane may be involved (Figure 11), although the hydrogen-bonding character of succinic acid is strongly directed along the $[10\bar{1}]_{sa}$ ledge.

In the case of 4-nitroaniline nucleation on L-valine, the $[10\bar{1}]_{pna}$–$[010]_{pna}$ and $[100]_{val}$–$[010]_{val}$ angles are both 90°, allowing alignment of these directions in the $(101)_{pna}$–$(001)_{val}$ interface. In the observed orientation the lattice mismatches are $[10\bar{1}]_{pna}$–$[010]_{val}$ = 3.88% and $[010]_{pna}$–$[100]_{val}$ = 37.5%. In contrast, the lattice mismatches of the unobserved orthogonal orientation are $[10\bar{1}]_{pna}$–$[100]_{val}$ = 27.6% and $[010]_{pna}$–$[010]_{val}$ = 15.2%. Therefore, 4-nitroaniline crystals adopt an orientation that allows the smallest lattice mismatch along at least one dimension, in this case along the $[010]_{val}$ ledge direction. However, examination of low-index 4-nitroaniline crystal planes that are paired with $(101)_{pna}$ and share $[10\bar{1}]_{pna}$ reveals that no pair has dihedral angles within 2° of the dihedral angle of the $[010]_{val}$ ledge site, even though growth on the ledge indicates that both planes of the ledge are important for nucleation. The lack of a suitable dihedral angle match suggests that the length scale of the interaction between the aggregate and the step plane along the height of the step may correspond to only a single or a few 4-nitroaniline chains. That is, nucleation may be driven by interfacial interaction of an aggregate consisting of 4-nitroaniline molecules assembled in a $[10\bar{1}]_{pna}$ chain with $(001)_{val}$ and $(\bar{2}01)_{val}$, the process favored by a reasonable lattice match over the length scale of the aggregate. Dipolar interactions may also contribute to the nucleation and orientation effects, as the polar 4-nitroaniline $[10\bar{1}]_{pna}$ chains and polar $(101)_{pna}$ layers are aligned along the polar $[010]_{val}$ direction. Contributions from this effect may be responsible for the morphology of the 4-nitroaniline crystals, which indicated more rapid growth along $[10\bar{1}]_{pna}$ relative to $[010]_{pna}$ compared to growth on succinic acid.

The examination of 4-nitroaniline nucleation was prompted by its significant molecular polarizability, which suggests promise for second harmonic generation, provided a noncentrosymmetric polymorph can be crystallized. It was anticipated that properly designed interfaces capable of hydrogen bonding or dipole–dipole interactions with the nucleant could direct the acentric 4-nitroaniline layers into a parallel motif, leading to nucleation of a noncentrosymmetric polymorph. Apparently, the dipolar forces between $(101)_{pna}$ layers in bulk 4-nitroaniline outweigh dipolar directing forces between the aggregate and the terrace and step planes, leading to the $P2_1/n$ phase. This is likely a consequence of the relatively poor lattice match along the $[10\bar{1}]_{pna}$–$[010]_{val}$ interface. The parallel orientation at the interface of the polar $(101)_{pna}$ layers with respect to the L-valine polar axis and the

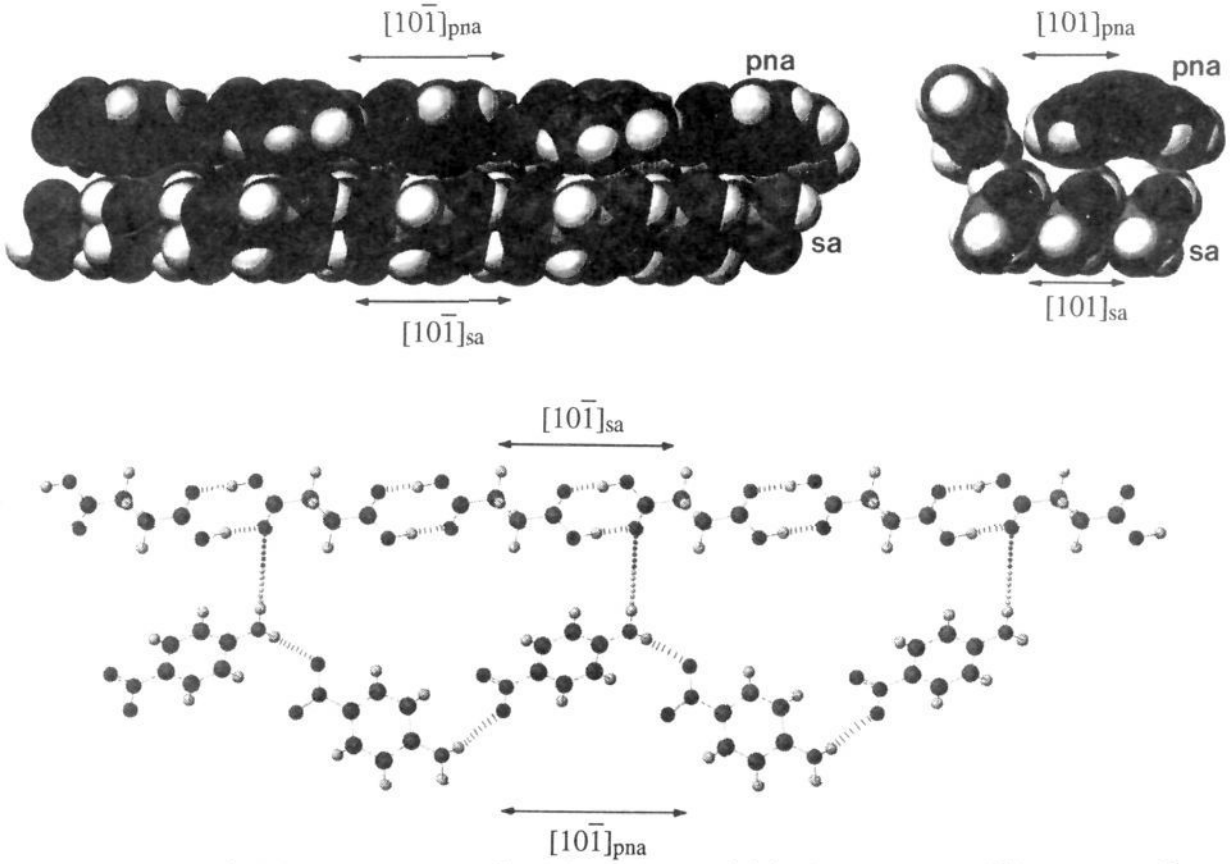

Figure 11. Representation of a hydrogen-bonded 4-nitroaniline chain nested in a $[101]_{sa}$ ledge site as viewed along $(0\bar{1}0)_{sa}$ normal to $[10\bar{1}]_{sa}$ (upper left) and along $(0\bar{1}0)_{sa}$ parallel to $[10\bar{1}]_{sa}$ (upper right). The molecular models suggest that interfacial interactions between the $(101)_{pna}$ plane of the 4-nitroaniline chain and $(010)_{sa}$ are dominated by dispersive forces. The bottom portion of the figure depicts the hydrogen-bonded 4-nitroaniline chain along $[10\bar{1}]_{pna}$ next to a chain of succinic acid molecules in the $\{111\}_{sa}$ step plane of the nucleating ledge site (the *b* axis is normal to the plane of the paper). Dispersive contacts between the $\{111\}_{sa}$ step plane and the "zigzag" 4-nitroaniline chains appear to be less significant, but hydrogen bonding between the free N–H of 4-nitroaniline and succinic acid carbonyl atoms on the $\{111\}_{sa}$ step plane is feasible. This suggests that 4-nitroaniline chains may be stabilized to some extent by hydrogen bonding.

$(001)_{val}$ surface, and the translation symmetry of the L-valine molecules in the $(001)_{val}$ layers exposed at the step plane may also play an important role. This has obvious implications for the design of solid interfaces for nucleation of noncentrosymmetric phases: the substrate should contain orienting dipoles or functional groups capable of orienting 4-nitroaniline layers *normal* to the nucleation interface.

The observation of nucleation predominantly at ledges on succinic acid and L-valine substrates and the relationships between the geometry of the $[10\bar{1}]_{sa}$ and $[010]_{val}$ ledge sites and the putative molecular planes of the benzoic acid and 4-nitroaniline aggregates suggest a nucleation mechanism in which mobile species (e.g., benzoic acid dimers or 4-nitroaniline molecules) adsorb on the substrate crystal planes, with subsequent condensation of these species, at the ledge site, into a prenucleation aggregate whose structure mimics that of the mature crystal (Figure 2, bottom). The hydrogen bonding groups of succinic acid and L-valine are involved in hydrogen bonding *within* the planes of the substrate ledge site, and the L-valine surfaces are hydrophobic, strongly suggesting that nondirectional dispersive forces primarily are responsible for stabilization of the prenucleation aggregate. In the case of benzoic acid, this would favor a nucleation mechanism involving benzoic acid hydrogen-bonded dimers instead of monomers. The stability of benzoic acid dimers is supported by spectroscopic evidence[42] and the high enthalpy of hydrogen bond formation (20–30 kJ/mol).[43] Van der Waals interactions between planar dimers, which contribute more than 40 kJ/mol per benzenoid ring in an organized lattice structure,[44] can result in the self-assembly at the ledge of benzoic acid molecules into stacks of dimers required for the aggregate structure. Similar arguments are valid for 4-nitroaniline, which is likely to self-assemble at the ledge into molecular hydrogen-bonded chains. After the aggregate reaches a critical size, nucleation and subsequent crystal growth can occur. The ledge-directed epitaxy mode of nucleation has the following features: (1) nucleation at a ledge site with a very small lattice mismatch along the ledge direction, (2) interfacial interaction of both planes of substrate ledges with two planes of the aggregate, the planes having small molecular corrugation, high packing density, and similar dihedral angles in order to maximize attractive interfacial interactions, (3) stabilization of prenucleation aggregates by dispersive forces (which are always attractive in a vacuum), with possible contributions from hydrogen bonding in the case of 4-nitroaniline, and (4) topographically directed growth orientation that is dictated by the orientation of the ledge site.

Thermodynamic Considerations: Dispersive vs Polar Interactions. The observations described above indicate that nucleation depends upon the substrate topography, crystallographic symmetry, and chemical composition of the substrate. While the terrace and step planes of the ledge site play an important role

(42) Bellamy, L. J. *The Infrared Spectra of Complex Organic Molecules*; John Wiley and Sons: New York, 1975. (b) Avram, M.; Mateescu, Gh. D. *Infrared Spectroscopy: Applications in Organic Chemistry*; Wiley-Interscience: New York, 1972.

(43) (a) Davies, M.; Jones, J. I. *Trans. Faraday Soc.* **1954**, 1042. (b) Pauling, L. *The Nature of the Chemical Bond*, 3rd ed.; Cornell University Press: Ithaca, NY, 1960; pp 477–478 and references therein. (c) Wall, F. T.; Rouse, P. R. *J. Am. Chem. Soc.* **1941**, *63*, 3002.

(44) Bradley, R. S.; Cleasby, T. G. *J. Chem. Soc.* **1952**, 1690.

in defining the nucleation mechanism and growth orientation on succinic acid and L-valine, the observation of low nucleation rates and random growth orientations on α-glycine and malonic acid suggests that nucleation and growth orientation is much less predominant on more polar substrate surfaces, even though the *a* and *c* lattice constants of α-glycine, which coincide with the ledge directions, are nearly identical to $[010]_{ba}$ and $[100]_{ba}$ (b = 5.14 Å; a = 5.52 Å), corresponding to lattice mismatches of 0.8% and 1.1%, respectively.[45] Similarly, nucleation of 4-nitroaniline on α-glycine or malonic acid did not occur readily and gave randomly oriented growth, even though $[10\bar{1}]_{pna}$ has only 0.5% and 1.71% lattice mismatch with the $[100]_{gly}$ and $[010]_{mal}$ ledges, respectively.

These results indicate that ledge-directed epitaxy is most significant when the substrate surfaces are relatively nonpolar, conditions that would favor the participation of *attractive* dispersive interactions between the growing phase and the substrate ledge site. *Under these conditions, the nondirectional nature of dispersive interactions would favor growth orientations dictated by the geometry of the ledge.* Strongly polar interfaces, or interfaces with specific molecular functionalities, may provide local orienting forces at the ledge site that would not necessarily correspond to ledge geometry and orientation. Additionally, in contrast to dispersive forces, polar interactions such as dipole–dipole or dipole–induced dipole interactions can be repulsive.

The role of different interaction energies in the nucleation process can be surmised by considering the interaction energy, $W(D)$, between a growing benzoic acid aggregate and a single crystal substrate using eq 5, in which an aggregate dimer stack

$$W(D) = -(ALR^{0.5})/(17D^{1.5}) \quad (5)$$

is modeled as a cylinder interacting with a planar substrate surface. In this equation, A is the Hamaker constant, L is the length of the dimer stack, R is the effective radius of the dimer, and D is the contact distance between aggregate and surface.[46] On the basis of molecular models of the benzoic acid dimer, R = 0.5 nm and D = 0.3 nm are reasonable values for our purposes. The Hamaker constant can be calculated with eq 6 where C_{vdw} is the

$$A = \pi^2 C_{vdw} \rho_1 \rho_2 \quad (6)$$

van der Waals coefficient and ρ_1 and ρ_2 are substrate and benzoic acid molecular densities in the solid state. C_{vdw} for disimilar molecules can be approximated by the sum of induction, orientation, and dispersion terms given by eqs 7–10, where u is

$$C_{vdw} = C_{ind} + C_{orient} + C_{disp} \quad (7)$$

$$C_{ind} = (u_1^2 \alpha_{o2} + u_2^2 \alpha_{o1})/(4\pi\epsilon_o)^2 \quad (8)$$

$$C_{orient} = [(u_1^2 u_2^2)/3kT]/(4\pi\epsilon_o)^2 \quad (9)$$

$$C_{disp} = [1.5\alpha_{o1}\alpha_{o2} I_1 I_2/(I_1 + I_2)]/(4\pi\epsilon_o)^2 \quad (10)$$

the experimental dipole moment,[47] α_o is the calculated molecular polarizability,[48] and I is the experimental ionization potential.[49]

The values of C_{ind} and C_{orient} obtained with eqs 8 and 9, commonly referred to as the Debye and Keesom interaction terms, respectively, are based on an assumption that the molecules behave as freely rotating dipoles.[50] While this may be a reasonable assumption for molecules adsorbing on the substrate surface from the gas phase, these relationships do not distinquish between the binding energies of different aggregate orientations on a substrate plane. Such considerations may be more relevant to the actual nucleation process, particularly when growth orientation effects are observed. We will consider both cases here, beginning with the freeely rotating dipole assumption.

Calculations based on freely rotating dipoles and benzoic acid monomers indicate that *dispersive interactions predominate for benzoic acid growth on* L-*valine and succinic acid substrates* (Table I).[51] For benzoic acid/succinic acid interactions, C_{orient} and C_{ind} have a negligible contribution (<3%) to C_{vdw}, implying that the observed crystal orientation effects result from dispersive interactions between the aggregate and the substrate ledge site. *Under these conditions, topographic effects resulting from ledge geometry and orientation would be expected to direct the growth orientation because dispersive forces are nondirectional.* The relative contribution of C_{ind} and C_{orient} to C_{vdw} increases to 19% for benzoic acid/L-valine, but these contributions decrease significantly if benzoic acid *dimers* (u = 0 D) are used for calculating the Hamaker constant instead of monomers. These calculations suggest that dispersive interactions are principally responsible for stabilizing benzoic acid aggregates at succinic acid and L-valine ledge sites.

Because of the strong dipole present in 4-nitroaniline, its crystal growth on succinic acid and L-valine will likely involve greater contributions from C_{ind} and C_{orient}. Indeed, the contribution of C_{ind} increases to 22% of C_{vdw} for 4-nitroaniline/succinic acid. However, it is reasonable to consider the observed orientation of the 4-nitroaniline crystals, which must necessarily reflect the orientation of the prenucleation aggregate. If the observed orientation is considered, the contribution of C_{ind} assuming that 4-nitroaniline is a fixed dipole and that succinic acid is a polarizable molecule may be estimated by eq 11, where θ represents the angle

$$C_{ind} = u_{pna}^2 \alpha_{osuc}(1 + 3\cos^2\theta)/2(4\pi\epsilon_o)^2 \quad (11)$$

$$C_{orient} = u_1 u_2 [2\cos\theta_1 \cos\theta_2 - \sin\theta_1 \sin\theta_2 \cos\phi]/4\pi\epsilon_o r^3 \quad (12)$$

between the 4-nitroaniline dipole axis and an axis connecting succinic acid and 4-nitroaniline molecules (Scheme I). Likewise, C_{orient} can be estimated for a fixed 4-nitroaniline dipole and a fixed substrate molecule dipole such as L-valine using eq 12, where θ_1 is the angle between the 4-nitroaniline and an axis connecting 4-nitroaniline and L-valine dipoles, θ_2 is the angle between the L-valine and an axis connecting 4-nitroaniline and L-valine dipoles, and ϕ is the dihedral angle between dipoles (Scheme II). Since the dipolar axis of the 4-nitroaniline molecules in the $[10\bar{1}]_{pna}$ chains lies parallel to $(111)_{sa}$ and $(0\bar{1}0)_{sa}$ in the observed orientation (θ = 90°), C_{ind} = 1.9 × 10^{-77} Jm^6. Under this condition, C_{disp} increases to 88% of C_{vdw}, substantially larger than the C_{disp} contribution for the freely rotating dipole assumption. Similar trends are observed for the interaction of 4-nitroaniline with L-valine. If the fixed dipole constraint is based on the observed growth orientation of 4-nitroaniline (θ_1 = 90°, θ_2 = 90°, ϕ =

(45) In the case of α-glycine, the $[100]_{gly}$–$[001]_{gly}$ angle (β = 111.7°), which is contained in the $(010)_{gly}$ plane, is 21.7° greater than the $[100]_{ba}$–$[010]_{ba}$ angle in $(001)_{ba}$. This would disfavor an epitaxially driven two-dimensional nucleation mechanism at the $(010)_{gly}$–$(001)_{ba}$ interface. A lattice match along $[010]_{gly}$, the agreement between the dihedral angles of glycine ledges (θ_{sub} values of the $[100]_{gly}$ and $[001]_{gly}$ ledges are 113° and 111.6°, respectively), and the low index planes in benzoic acid and 4-nitroaniline would appear to favor the ledge directed epitaxy mechanism.

(46) Israelachvili, J. *Intermolecular and Surface Forces*; Academic Press: New York, 1992; pp 44–212.

(47) McClellan, A. L. *Table of Experimental Dipole Moments*; W. H. Freeman and Co.: San Francisco, 1963.

(48) Molecular polarizabilities were calculated on the basis of procedures described in ref 46, Chapter 5.

(49) Lias, S. G.; Bartmess, J. E.; Liebman, J. F.; Holmes, J. L.; Levin, R. D.; Mallard, W. G. *J. Phys. Chem. Ref. Data* **1988**, *17*, Supplement. No. 1 (American Chemical Society and the American Institute of Physics).

(50) These values, which describe the angle-averaged potentials (averaged over all space), are not zero because of a Boltzmann weighting factor that assigns more weight to the lower energy orientations. The freely rotating dipole assumption generally is most valid at large separations or in a medium of large ϵ, where the angle dependence of the interaction energy falls below kT.

(51) Details of the calcuations, including the values of u, α_o, and I used to obtain the coefficients in Table I, are available from the authors upon request.

Table I. Van der Waals Coefficients, C (% of C_{vdw}), and Hamaker Constants, A[a]

substrate	molecule	C_{ind} (10^{-78} J m^6)	C_{orient} (10^{-78} J m^6)	C_{disp} (10^{-78} J m^6)	C_{vdw} (10^{-78} J m^6)	A (10^{-20} J)
succinic acid	benzoic acid monomer freely rotating	3 (2%)	0 (0%)	130 (98%)	133	6.8
	benzoic acid dimer freely rotating	0	0	260 (100%)	260	6.6
	benzoic acid dimer fixed dipole[c]	0	0	260 (100%)	260	6.6
	4-nitroaniline monomer freely rotating	39 (22%)	0 (0%)	140 (78%)	179	8.8
	4-nitroaniline monomer fixed dipole[c]	19 (12%)	0 (0%)	140 (88%)	159	7.8
L-valine	benzoic acid monomer freely rotating	15 (8%)	21 (11%)	160 (81%)	196	8.2
	benzoic acid dimer freely rotating	23 (7%)	0 (0%)	320 (93%)	343	7.1
	benzoic acid dimer fixed dipole[c]	6.4 (2%)	0 (0%)	320 (98%)	326	6.8
	4-nitroaniline monomer freely rotating	64 (10%)	310 (48%)	270 (42%)	644	26
	4-nitroaniline monomer fixed dipole[b,c]	37 (10%)	±53 (15%)[d]	270 (75%)	360	14
α-glycine	benzoic acid monomer freely rotating	510 (33%)	930 (61%)	87 (6%)	1527	81
	benzoic acid dimer freely rotating	1014 (85%)	0 (0%)	174 (15%)	1188	32
malonic acid	4-nitroaniline monomer freely rotating	43 (11%)	230 (59%)	120 (30%)	393	20

[a] Dipole moments, calculated polarizabilities, and ionization potentials were obtained from literature sources; a listing is available from the authors upon request. [b] u_{val} determined from the crystal structure. [c] The observed growth orientation was used for calculation of the fixed dipole values of C_{ind} and C_{orient} at $R = 0.3$ nm. [d] The sign of the interaction depends upon whether the dipole 4-nitroaniline chains are oriented parallel or antiparallel to the polar axis of L-valine.

Scheme I

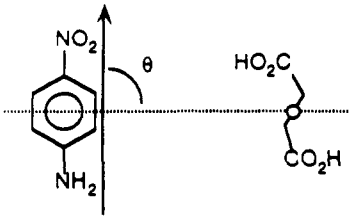

Scheme II

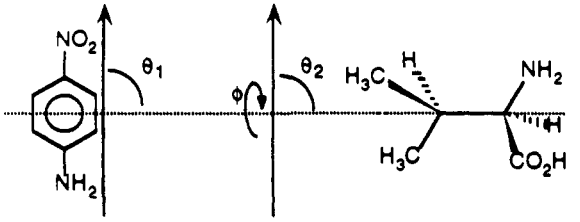

26°), a reduction in C_{orient} results in an increase in the contribution of C_{disp} from 42% for the freely rotating dipole condition to 75%. The calculations therefore support the importance of dispersive forces in nucleation, although the lesser contributions of polar terms can influence the orientation of the crystals. We note that these calculations do not take into account hydrogen-bonding effects discussed earlier, which also may increase the tendency of 4-nitroaniline chains to assemble in the observed orientations.

The benzoic acid/α-glycine and 4-nitroaniline/malonic acid interactions involve rather large dipole and induced dipole contributions to the van der Waals interactions (Table I). The absence of growth orientation effects in these examples precluded estimates of the van der Waals interaction based on fixed dipoles. However, comparison of the freely rotating C_{ind} and C_{orient} values with the corresponding values for the less polar succinic acid and L-valine substrates indicates a substantially larger contribution of C_{ind} and C_{orient} to C_{vdw} for α-glycine and malonic acid. While dispersive forces are always attractive, this is not necessarily the case for the Debye and Keesom interactions. Larger freely

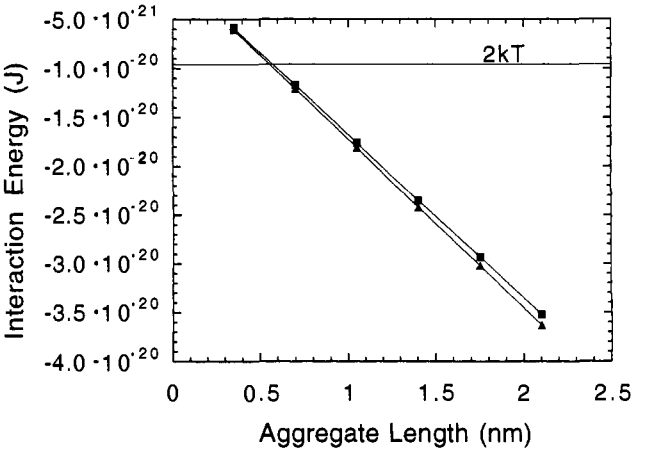

Figure 12. The interaction energy, W(D), as a function of benzoic acid dimer stacking length, L, on succinic acid (▲) and L-valine (■). For each dimer, L is incremented by 0.35 nm. The binding energy of an aggregate exceeds $2kT$ at three benzoic acid dimers (L = 1.05 nm).

rotating C_{ind} and C_{orient} values therefore may be manifested as repulsive interactions between benzoic acid or 4-nitroaniline aggregates and these substrates, increasing the likelihood of interfaces that are unfavorable for nucleation. Under these conditions, higher driving forces would be required for nucleation and random growth orientations would be expected. Strong dipolar contributions also can lead to growth orientations that are unrelated to the ledge orientation, as was experimentally observed for these polar substrates.

The binding energy of benzoic acid aggregates with succinic acid and L-valine substrates, as a function of aggregate length, L, can be estimated (Figure 12). These calculations indicate that W exceeds $2kT$ for an aggregate structure consisting of three stacked dimers (L = 1.1 nm). The relatively short length scale of these aggregates suggests that small lattice mismatches at the ledge site can be tolerated. It should be noted that W values for benzoic acid/succinic acid or benzoic acid/L-valine interactions are nearly identical, which can be attributed to nearly identical

($C_{vdw}\rho$) values. These calculations do not take into account interdimer interactions (i.e., ΔG_V); therefore, this value is probably very conservative. This approach does not account for many-body interactions, which can lead to errors in the estimated van der Waals energies approaching 20%. Nevertheless, some important points can be made about the role of dispersive forces: (1) at a ledge site, the presence of another substrate crystallographic plane within van der Waals contact distance will effectively double W; (2) crystallographic planes with higher molecular packing densities at the interface will lead to a more favorable W, and planes which are topographically mismatched (differing molecular corrugations) will have a larger average D resulting in a less favorable W; (3) angular match of crystallographic planes at a ledge site will result in a smaller value of D, leading to a more favorable W. A one-dimensional lattice match along the ledge direction would further enhance interactions between contacting planes. While this model does not discriminate between different ledge geometries or crystal orientations, it does provide a framework for understanding aggregate adsorption at single crystal ledge sites as well as estimates of the critical prenucleation aggregate size.

Conclusions

Nucleation of benzoic acid from the gas phase is promoted by surfaces of molecular single crystals that can stabilize molecular prenucleation aggregates via a unique topographically directed epitaxy mechanism that involves interaction of the aggregates with specific, crystallographically well defined ledge sites on the substrate. The predominance of crystal growth on ledges demonstrates that nucleation preferentially occurs when the prenucleation aggregate can interact with two crystal planes. The nucleation behavior is consistent with a ledge directed epitaxy involving a one-dimensional lattice match along the ledge and a ledge geometry that is complementary to that of the prenucleation aggregate. Nucleation occurs at these ledge sites under conditions of significantly less driving force than those required for crystal growth on nonpromoting solid substrates. The observation of crystal growth at well-defined ledge sites can be explained on the basis of aggregates with supramolecular structure identical to that of the mature crystal, supporting the premise that prenucleation aggregates resemble the mature crystal. Ledge-directed epitaxy is observed when the crystallographic planes of the substrate and aggregate have high packing densities and low molecular corrugation, and when the interfacial interactions predominantly involve nondirectional dispersive forces, which are always attractive in vacuum. Conversely, crystal substrates with large dipolar contributions render nucleation less favorable and topographic orientation effects less likely.

The unique ability of these molecular crystal substrates to direct crystal growth is a consequence of well-defined crystal planes that are not present in amorphous, macroscopic surface-relief structures such as those used in graphoepitaxy, a process where macroscopic surface relief structure provides interfacial stabilization of nuclei during crystallization.[52] Proper choice of molecular crystal substrates can provide a range of surface relief structures in which topography and molecular structure can be tailored for the aggregate morphology, thereby influencing nucleation and crystal orientation in a controlled manner.

The active substrate ledges are the preferred site for nucleation even when unit cell lattice constants in the active interface appear to be epitaxially matched with an alternative orientation. These studies illustrate that the design of substrate-promoted crystal growth processes based on simple epitaxy models involving matching of unit cell lattice directions may not be appropriate in many circumstances. It is evident that molecular crystal substrates provide unique opportunities to examine some of the critical factors responsible for nucleation and that surface topography needs to be considered in crystal growth processes occurring on heterogeneous substrates. We anticipate that further studies, including extension of these principles to nucleation and growth in solutions, will provide substantial insight into behavior such as crystal growth seeding, crystal morphology, and selectivity toward polymorphs during the crystal growth process.

Acknowledgment. The authors gratefully acknowledge the support of the National Science Foundation (NSF/DMR-9107179) and the Center for Interfacial Engineering (NSF Engineering Research Centers Program, CDR 8721551). The authors also are grateful for the assistance of Prof. Doyle Britton with X-ray crystallographic analyses and Mr. A. C. Hillier for SEM characterization of AFM tips.

Supplementary Material Available: Three tables of ledge lengths and dihedral angles for various low-index planes of the substrates and nucleants (3 pages). Ordering information is given on any current masthead page.

(52) (a) Smith, H. I.; Flanders, D. C. *Appl. Phys. Lett.* **1978**, *32*, 349. (b) Geis, M. W.; Flanders, D. C.; Smith, H. I. *Appl. Phys. Lett.* **1979**, *35*, 71. (c) Anton, R.; Poppa, H.; Flanders, D. C. *J. Cryst. Growth* **1982**, *56*, 433.